JOURNAL OF THE AERONAUTICAL SCIENCES

VOLUME 9 OCTOBER, 1942 NUMBER 12

Vector Methods of Flutter Analysis

WILLIAM M. BLEAKNEY* AND J. DOUGLAS HAMM†

Lockheed Aircraft Corporation

ABSTRACT

The application of vector notation to generalized flutter equations is described, and the advantages of graphic stability solutions are pointed out. The expressions for three-dimensional aerodynamic and mechanical coefficients are given. The use of stability curves in the presentation of data and the interpretation of these curves in terms of flutter characteristics are explained.

For solving the determinantal equation analytically, a convenient method of successive reduction in order is presented. In graphic solutions certain circle relationships have been found useful; when applied to determinantal elements, these relationships form the basis of solutions developed in two and three degrees of freedom.

The analysis of a symmetric flutter mode of a twin-fin tail is outlined to illustrate the methods of solution described. Actual examples of the evaluation of parameters are given and a circle diagram is applied to the solution of the stability equation. The circle diagram and a two-degree-of-freedom M-curve are used to determine the effects upon flutter characteristics of variations in parameters.

The simplifying assumptions as applied to different problems vary widely. Likewise, variations in the detailed graphic operations are used, depending upon the nature of the data and the information desired.

INTRODUCTION

THERE HAS previously been developed a flutter stability equation in generalized coordinates which is applicable to any number of degrees of freedom.[1] Occasionally, it is desirable to solve this equation for as many as four or five degrees of freedom, but for most routine problems only two or three degrees of freedom need be considered simultaneously. As might be expected, the labor required in setting up and in solving the equation increases rapidly with the order of the determinant.

Because of assumptions made or because of lack of information, some of the flutter parameters are often somewhat uncertain. Other parameters actually vary under different flight conditions. It is important, then, that the methods of solution employed permit evaluation of errors and estimation of the effects of changes in parameters.

In the calculation of the stability determinant considerable labor is saved by expressing the complex elements in terms of magnitude and angle rather than as real and imaginary numbers. With the aid of a few simple geometric relationships these vectors are handled by graphic methods whenever possible. Thus, well-known advantages in making rapid approximate calculations, in eliminating large errors, in estimating accuracy, and in providing the analyst with a feeling for general effects are utilized. Similar methods have been applied to specific types of problems by Kassner and Fingado,[2] Bergen and Arnold,[3] and Arnold.[4] Except in the last case, however, these methods do not appear suitable for three-dimensional problems, and in the last case a change in the value of a parameter would seem to require almost a complete repetition of the solution.

The vector methods of analysis presented here have been made applicable to as large a variety of problems as possible. Based upon a single set of aerodynamic coefficient plots, they eliminate virtually all other preliminary work, such as development of specialized charts. Most important, the methods have been designed to meet the requirements mentioned above. They are applicable to any number of degrees of freedom, they allow ready estimation of errors, and they permit rapid evaluation of the effects of changes in parameters.

SYMBOLS

A_{ij}	= aerodynamic force coefficient
b	= airfoil half-chord
b_0	= reference half-chord
c	= distance from airfoil mid-chord to control-surface hinge, as a fraction of b
c_1	= distance from airfoil quarter-chord line to control-surface hinge
D_{ij}	= diameter of circle expressed as a complex vector

Received March 16, 1942.

* Research Engineer.

† Junior Research Engineer.

F_i = structural force coefficient
f_i = normalized deflection mode
g_i = structural damping coefficient expressed as a fraction of stiffness
h_i = value of f_i at quarter-chord line
I_{ij} = imaginary part of vector V_{ij}
i = $\sqrt{-1}$
i, j = general subscripts indicating deflection modes
k = reduced frequency ($= b\omega/v$)
k_0 = reduced frequency referred to b_0
M_{ij} = mechanical force coefficient
m_{ij} = inertia term
n = number of degrees of freedom
R_{ij} = real part of vector V_{ij}
r = distance aft of control surface hinge
r_0 = radius of gyration of total airfoil section about its center of gravity
r_β = radius of gyration of control-surface section about its hinge
S = reference span
V_{ij} = vector in the complex plane
V_P = product vector
v = true air speed ($= v_0/k\sqrt{X}$)
v_0 = reference speed ($= \omega_0 b_0$)
X = flutter frequency parameter ($= \omega_0^2/\omega^2$)
x = chordwise coordinate measured aft from quarter-chord
x_e = x-coordinate of total airfoil section shear center or elastic axis
x_0 = x-coordinate of total airfoil section center of gravity
x_β = distance from hinge to center of gravity of control-surface section
y = spanwise coordinate
z = spanwise coordinate of vertical surfaces
α_i, β_i = weighting factors
ρ = air density
ρ_0 = air density at sea level
θ_{ij} = angle of vector V_{ij}
Ω_{ij} = structural coupling term
Ω_i = primitive frequency parameter ($= \omega_i^2/\omega_0^2$)
ω = circular flutter frequency
ω_i = natural or primitive frequency of the mode f_i
ω_0 = reference frequency
Δy = element of span of airfoil
Δm = mass of airfoil segment Δy
Δm_β = mass of control-surface segment Δy

Vectorial Determinant Elements

The general equation for flutter stability is expressed[1] by the following determinant:

$$\begin{vmatrix} A_{11}+M_{11} & A_{12}+M_{12} & \cdots & A_{1n}+M_{1n} \\ A_{21}+M_{21} & A_{22}+M_{22} & \cdots & A_{2n}+M_{2n} \\ \cdot & \cdot & & \cdot \\ \cdot & \cdot & & \cdot \\ \cdot & \cdot & & \cdot \\ A_{n1}+M_{n1} & A_{n2}+M_{n2} & \cdots & A_{nn}+M_{nn} \end{vmatrix} = 0 \quad (1)$$

The three-dimensional aerodynamic coefficients in this equation are given by the general expression

$$A_{ij} = \Sigma[\alpha_i'\alpha_j''A_{a\alpha} + \alpha_i'h_j''A_{ah} + \alpha_i'\beta_j''A_{a\beta} + h_i'\alpha_j''A_{c\alpha} + h_i'h_j''A_{ch} + h_i'\beta_j''A_{c\beta} + \beta_i'\alpha_j''A_{b\alpha} + \beta_i'h_j''A_{bh} + \beta_i'\beta_j''A_{b\beta}](\Delta y/S) \quad (2)$$

Since this paper will be concerned with only a few of the more common flutter examples, the tab functions have been omitted from Eq. (2). The drag term, being of little importance, has also been omitted.

The two-dimensional A's in Eq. (2) are Theodorsen's coefficients[5] with the mechanical terms omitted. In the present development the choice of a value of Theodorsen's a in these expressions is completely arbitrary and amounts to choosing a reference axis for defining moment coefficients and normal displacements. Some of the aerodynamic coefficients, notably A_{ah} and $A_{a\alpha}$, assume particularly simple forms if the quarter-chord line is used for this purpose; accordingly, a is put equal to $-1/2$, and the following expressions are obtained for the real and imaginary parts:

$$R_{a\alpha} = -3/8 \qquad I_{a\alpha} = 1/k$$

$$R_{a\beta} = \frac{T_7}{\pi} + (c + 1/2)\frac{T_1}{\pi} + \frac{1}{k^2}\left(\frac{T_4}{\pi} + \frac{T_{10}}{\pi}\right)$$

$$I_{a\beta} = (1/k)[-(2p/\pi) - (T_4/\pi)]$$

$$R_{ah} = -1/2 \qquad I_{ah} = 0$$

$$R_{b\alpha} = \frac{T_7}{\pi} + (c + 1/2)\frac{T_1}{\pi} - \frac{1}{k}\frac{T_{12}}{\pi}G + \frac{T_{12}}{\pi}\frac{F}{k^2}$$

$$I_{b\alpha} = \frac{1}{k}\left[\frac{T_{12}}{\pi}F + \frac{T_{12}}{\pi}\frac{1}{k}G + \left(\frac{P}{\pi} - \frac{T_1}{\pi} - \frac{T_4}{2\pi}\right)\right]$$

$$R_{b\beta} = \frac{T_3}{\pi^2} + \frac{1}{k^2}\left(\frac{T_5}{\pi^2} - \frac{T_4T_{10}}{\pi^2}\right) - \frac{T_{12}T_{11}}{2\pi^2}\frac{1}{k}G + \frac{T_{12}T_{10}}{\pi^2}\frac{F}{k^2}$$

$$I_{b\beta} = \frac{1}{k}\left[\frac{T_{12}T_{11}}{2\pi^2}F + \frac{T_{12}T_{10}}{\pi^2}\frac{1}{k}G - \frac{T_4T_{11}}{2\pi^2}\right]$$

$$R_{bh} = (T_1/\pi) - [(T_{12}/\pi)(1/k)G]$$

$$I_{bh} = (1/k)(T_{12}/\pi)F$$

$$R_{c\alpha} = -1/2 - 2(1/k)G + 2F/k^2$$

$$I_{c\alpha} = (1/k)[2F + 2(1/k)G + 1]$$

$$R_{c\beta} = \frac{T_1}{\pi} - \frac{T_{11}}{\pi}\frac{1}{k}G + 2\frac{T_{10}}{\pi}\frac{F}{k^2}$$

$$I_{c\beta} = \frac{1}{k}\left[\frac{T_{11}}{\pi}F + 2\frac{T_{10}}{\pi}\frac{1}{k}G - \frac{T_4}{\pi}\right]$$

$$R_{ch} = -1 - 2(1/k)G \qquad I_{ch} = (1/k)2F$$

The parameters in these equations have been defined and tabulated by Theodorsen and Garrick.[6] Numerical values of the coefficients are given in Tables 1 to 8. It is again emphasized that coefficients based on any other reference axis besides the quarter-chord line are obtained from these in accordance with Eq. (2).

In many airplane flutter problems, particularly when the taper of the surface over the span to be considered is slight and an effective rectangular planform can be assumed, the two-dimensional coefficients appear singly or in simple combinations in the elements of the determinant. For these problems, the aero-

TABLE 1

Two-Dimensional Aerodynamic Coefficients Independent of c

$1/k$	k	k^2	$R_{a\alpha}$	$I_{a\alpha}$	R_{ah}	I_{ah}	$R_{c\alpha}$	$I_{c\alpha}$	R_{ch}	I_{ch}
0	∞	∞	−0.375	0	−0.50	0	−0.5	0	−1	0
0.5	2	4	−0.375	0.5	−0.50	0	−0.186	0.984	−0.942	0.513
0.833	1.2	1.44	−0.375	0.833	−0.50	0	0.382	1.595	−0.854	0.883
1.25	0.8	0.64	−0.375	1.25	−0.50	0	1.523	2.271	−0.709	1.385
1.667	0.6	0.36	−0.375	1.667	−0.50	0	3.175	2.832	−0.541	1.929
2.0	0.5	0.25	−0.375	2.0	−0.50	0	4.886	3.186	−0.397	2.392
2.5	0.4	0.16	−0.375	2.5	−0.50	0	8.138	3.563	−0.175	3.125
2.941	0.34	0.1156	−0.375	2.941	−0.50	0	11.714	3.741	0.022	3.805
3.333	0.30	0.09	−0.375	3.333	−0.50	0	15.473	3.783	0.195	4.432
4.167	0.24	0.0576	−0.375	4.167	−0.50	0	25.319	3.524	0.552	5.824
5.0	0.20	0.04	−0.375	5.00	−0.50	0	37.766	2.846	0.886	7.276
6.25	0.16	0.0256	−0.375	6.250	−0.50	0	61.437	1.129	1.345	9.535
8.333	0.12	0.0144	−0.375	8.333	−0.50	0	114.49	−3.245	2.002	13.438
10.0	0.10	0.010	−0.375	10.0	−0.50	0	169.35	−7.820	2.446	16.640
12.5	0.08	0.0064	−0.375	12.5	−0.50	0	272.41	−16.115	3.010	21.510
16.667	0.06	0.0036	−0.375	16.667	−0.50	0	499.85	−32.817	3.753	29.733
20	0.05	0.0025	−0.375	20.0	−0.50	0	731.92	−48.040	4.220	36.360
25	0.04	0.0016	−0.375	25.0	−0.50	0	1,163.6	−73.665	4.800	46.335
40	0.025	0.000625	−0.375	40.0	−0.50	0	3,060.9	−162.68	5.976	76.360
100	0.01	0.0001	−0.375	100.0	−0.50	0	19,657	−667.52	8.640	196.48
∞	0	0	−0.375	∞	−0.50	0	∞	−∞	∞	∞

TABLE 2

Two-Dimensional Aerodynamic Coefficients, $c = 0$

$1/k$	$R_{a\beta}$	$I_{a\beta}$	$R_{b\alpha}$	$I_{b\alpha}$	$R_{b\beta}$	$I_{b\beta}$	R_{bh}	I_{bh}	$R_{c\beta}$	$I_{c\beta}$
0	−0.169	0	−0.169	0	−0.082	0	−0.212	0	−0.212	0
0.5	−0.089	0.356	−0.147	0.211	−0.051	0.160	−0.208	0.035	+0.030	0.518
0.833	+0.052	0.594	−0.108	0.349	+0.005	0.264	−0.202	0.060	0.473	0.819
1.25	0.329	0.890	−0.030	0.515	+0.115	0.389	−0.192	0.095	1.370	1.114
1.667	0.716	1.187	+0.082	0.673	0.274	0.506	−0.181	0.132	2.680	1.304
2.0	1.105	1.424	0.199	0.793	0.437	0.594	−0.171	0.163	4.045	1.373
2.5	1.821	1.781	0.421	0.963	0.744	0.716	−0.156	0.213	6.650	1.338
2.941	2.585	2.095	0.666	1.102	1.077	0.815	−0.142	0.260	9.527	1.173
3.333	3.368	2.374	0.923	1.218	1.425	0.897	−0.131	0.303	12.560	0.927
4.167	5.358	2.968	1.595	1.440	2.326	1.049	−0.106	0.398	20.528	0.102
5.0	7.789	3.561	2.445	1.633	3.452	1.176	−0.083	0.497	30.630	−1.082
6.25	12.265	4.451	4.062	1.876	5.570	1.327	−0.052	0.651	49.886	−3.449
8.333	21.936	5.935	7.687	2.177	10.259	1.491	−0.007	0.918	93.137	−8.668
10.0	31.662	7.122	11.434	2.344	15.062	1.561	0.023	1.137	137.92	−13.742
12.5	49.567	8.903	18.474	2.497	24.025	1.585	0.062	1.469	222.11	−21.751
16.667	88.250	11.870	34.024	2.555	43.673	1.462	0.112	2.031	408.04	−39.602
20	127.155	14.244	49.863	2.474	63.603	1.259	0.144	2.484	597.83	−54.780
25	198.775	17.805	79.351	2.163	100.57	0.797	0.184	3.165	951.56	−79.838
40	509.127	28.488	208.96	0.399	262.26	−1.268	0.264	5.216	2,503.1	−164.97
100	3,182.9	71.220	1,342.7	−16.818	1,669.4	−17.845	0.446	13.422	16,083.5	−627.27
∞	∞	∞	∞	−∞	∞	−∞	∞	∞	∞	−∞

dynamic coefficients are permanently plotted on a scale convenient for measuring vectors. Typical curves of this type are shown in Fig. 1. Values of the independent variable $1/k$ are shown along the curves. All coefficients relating to control surfaces vary with c, the hinge location parameter, and so are represented by families of curves, as in Fig. 1b. The control-surface hinge-moment coefficients (those having the subscript b) are generally multiplied by $2/(1 - c)^2$ for convenience in plotting, since this factor brings the curves of each family to the same order of magnitude. The coefficients thus revised are designated $A_{b\alpha}'$, A_{bh}', and $A_{b\beta}'$.

When taper is to be taken into account, the parameter k varies over the span in proportion to the chord. The summation in Eq. 2 is then carried out separately for the real and imaginary components, and the resulting three-dimensional coefficients are plotted and used in the same manner as the two-dimensional functions.

The mechanical coefficients of the stability determinant are defined[1] as

$$M_{ij} = -m_{ij}[1 - \Omega_{ij}X(1 + ig_{ij})] \qquad (3)$$

TABLE 3

Two-Dimensional Aerodynamic Coefficients, $c = 0.1$

$1/k$	$R_{a\beta}$	$I_{a\beta}$	$R_{b\alpha}$	$I_{b\alpha}$	$R_{b\beta}$	$I_{b\beta}$	R_{bh}	I_{bh}	$R_{c\beta}$	$I_{c\beta}$
0	−0.135	0	−0.135	0	−0.054	0	−0.165	0	−0.165	0
0.5	−0.048	0.323	−0.118	0.165	−0.029	0.118	−0.162	0.026	0.064	0.446
0.833	+0.107	0.538	−0.089	0.272	+0.016	0.195	−0.158	0.046	0.484	0.699
1.25	+0.410	0.807	−0.030	0.402	0.106	0.286	−0.150	0.072	1.337	0.936
1.667	0.833	1.076	+0.055	0.525	0.234	0.373	−0.142	0.100	2.583	1.068
2.0	1.259	1.291	0.144	0.619	0.366	0.438	−0.134	0.124	3.883	1.094
2.5	2.043	1.614	0.312	0.753	0.613	0.528	−0.123	0.162	6.369	0.998
2.941	2.879	1.898	0.497	0.862	0.882	0.593	−0.113	0.197	9.117	0.782
3.333	3.736	2.151	0.691	0.954	1.161	0.660	−0.104	0.229	12.016	0.486
4.167	5.914	2.689	1.220	1.130	1.885	0.772	−0.085	0.301	19.638	−0.414
5.0	8.575	3.227	1.843	1.284	2.788	0.866	−0.068	0.376	29.307	−1.667
6.25	13.474	4.034	3.066	1.480	4.482	0.978	−0.044	0.493	47.749	−4.120
8.333	24.059	5.379	5.808	1.727	8.227	1.100	−0.010	0.695	89.193	−9.438
10.0	34.704	6.454	8.643	1.870	12.057	1.153	0.013	0.860	132.12	−14.558
12.5	54.301	8.068	13.969	2.010	19.196	1.173	0.042	1.112	212.83	−23.385
16.667	96.641	10.757	25.992	2.094	34.829	1.088	0.080	1.537	391.11	−40.384
20	139.221	12.909	37.716	2.066	50.672	0.944	0.104	1.879	573.11	−55.459
25	217.609	16.136	60.026	1.878	80.042	0.614	0.134	2.395	912.36	−80.272
40	557.289	25.818	158.075	0.689	208.41	−0.870	0.195	3.946	2,400.4	−164.27
100	3,483.6	64.544	1,015.76	−11.756	1,324.6	−12.839	0.333	10.154	15,425	−617.03
∞	∞	∞	∞	−∞	∞	−∞	∞	∞	∞	−∞

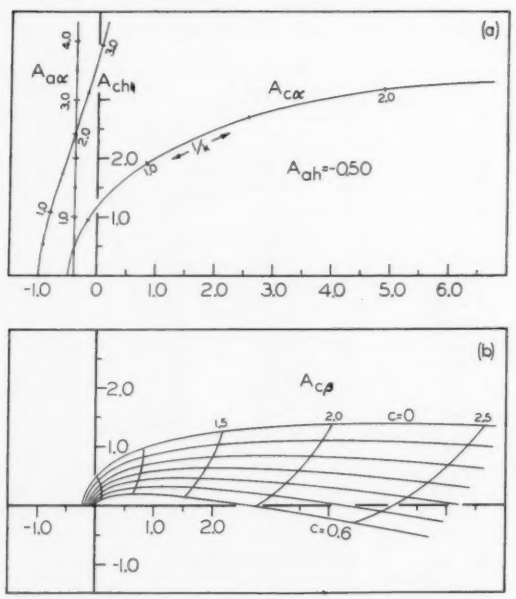

FIG. 1. Typical two-dimensional aerodynamic coefficients.

where

$$m_{ij} = \frac{1}{\pi\rho b_0^2 S}\sum\left\{\left[\frac{x_0^2 + r_0^2}{b_0^2}\alpha_i\alpha_j + \frac{x_0}{b_0}(\alpha_i h_j + h_i\alpha_j) + h_i h_j\right]\Delta m + \left[\frac{c_i x_\beta + r_\beta^2}{b_0^2}(\alpha_i\beta_j + \beta_i\alpha_j) + \frac{x_\beta}{b_0}(\beta_i h_j + h_i\beta_j) + \frac{r_\beta^2}{b_0^2}\beta_i\beta_j\right]\Delta m_\beta\right\} \quad (4)$$

Thus, when there is no damping, the mechanical terms are entirely real.

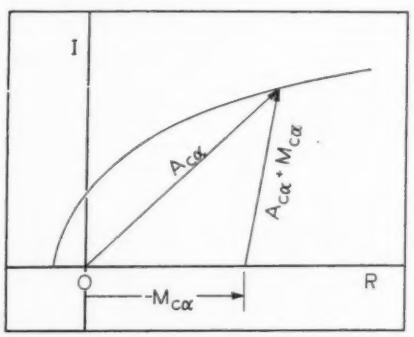

FIG. 2. Vectorial determination of a determinant element.

When vector notation is employed, any determinant element $A_{ij} + M_{ij}$ is expressed by a single vector and can be found in a single operation through use of a scale and protractor. As an example, Fig. 2 shows how the element $A_{c\alpha} + M_{c\alpha}$ is measured; the operation is the same for the other coefficients.

THE STABILITY CURVE

The vectors representing the determinant elements vary with both k_0 and X. For a given value of k_0 the stability determinant becomes a complex equation determining two quantities, one of which is the unknown X. For the other unknown it is convenient to choose one of the structural damping coefficients g_i. Both X and g_i can then be considered as functions of k_0.

The curve showing g_i as a function of $1/k_0\sqrt{X}$ or of the true air speed is called the "stability curve"; it indicates the damping necessary to maintain steady-state oscillations at any speed. If a horizontal line is drawn to indicate the true damping coefficient of the structure

TABLE 4

Two-Dimensional Aerodynamic Coefficients, $c = 0.2$

$1/k$	$R_{a\beta}$	$I_{a\beta}$	$R_{b\alpha}$	$I_{b\alpha}$	$R_{b\beta}$	$I_{b\beta}$	R_{bh}	I_{bh}	$R_{c\beta}$	$I_{c\beta}$
0	−0.104	0	−0.104	0	−0.034	0	−0.125	0	−0.125	0
0.5	−0.011	0.287	−0.092	0.124	−0.015	0.084	−0.123	0.019	0.091	0.376
0.833	+0.156	0.478	−0.071	0.205	+0.021	0.138	−0.119	0.033	0.486	0.584
1.25	0.481	0.716	−0.027	0.304	0.092	0.203	−0.114	0.053	1.290	0.765
1.667	0.935	0.955	+0.035	0.397	0.193	0.265	−0.107	0.073	2.469	0.839
2.0	1.393	1.146	0.100	0.469	0.296	0.311	−0.102	0.091	3.700	0.830
2.5	2.235	1.433	0.223	0.570	0.490	0.375	−0.094	0.119	6.057	0.677
2.941	3.133	1.686	0.359	0.653	0.701	0.426	−0.086	0.144	8.665	0.417
3.333	4.054	1.910	0.502	0.723	0.919	0.469	−0.080	0.168	11.418	0.091
4.167	6.393	2.388	0.875	0.858	1.484	0.548	−0.066	0.221	18.660	−0.883
5.0	9.252	2.866	1.347	0.978	2.188	0.615	−0.053	0.276	27.856	−2.190
6.25	14.516	3.582	2.245	1.169	3.506	0.694	−0.036	0.362	45.402	−4.702
8.333	25.886	4.776	4.257	1.326	6.413	0.781	−0.011	0.510	84.855	−10.065
10.0	37.322	5.731	6.338	1.443	9.382	0.819	+0.006	0.631	125.72	−15.187
12.5	58.374	7.164	10.247	1.563	14.909	0.835	0.028	0.816	202.61	−23.963
16.667	103.857	9.552	18.874	1.654	26.992	0.779	0.055	1.128	372.43	−40.777
20	149.600	11.463	27.675	1.656	39.231	0.681	0.073	1.379	545.81	−55.639
25	233.809	14.328	44.049	1.555	61.924	0.453	0.095	1.758	868.43	−80.027
40	598.716	22.925	116.01	0.787	161.00	−0.574	0.140	2.896	2,286.7	−162.30
100	3,742.5	57.313	745.50	−7.925	1,021.6	−8.903	0.241	7.452	14,697	−602.67
∞	∞	∞	∞	−∞	∞	−∞	∞	∞	∞	−∞

TABLE 5

Two-Dimensional Aerodynamic Coefficients, $c = 0.3$

$1/k$	$R_{a\beta}$	$I_{a\beta}$	$R_{b\alpha}$	$I_{b\alpha}$	$R_{b\beta}$	$I_{b\beta}$	R_{bh}	I_{bh}	$R_{c\beta}$	$I_{c\beta}$
0	−0.077	0	−0.077	0	−0.020	0	−0.091	0	−0.091	0
0.5	0.021	0.247	−0.069	0.091	−0.005	0.057	−0.089	0.014	+0.110	0.309
0.833	0.197	0.412	−0.054	0.150	+0.022	0.094	−0.087	0.024	0.479	0.473
1.25	0.539	0.618	−0.023	0.222	+0.076	0.138	−0.083	0.037	1.232	0.602
1.667	1.019	0.823	+0.021	0.291	0.154	0.179	−0.078	0.052	2.338	0.633
2.0	1.502	0.988	+0.067	0.343	0.233	0.210	−0.074	0.064	3.494	0.582
2.5	2.390	1.235	0.154	0.417	0.380	0.253	−0.069	0.084	5.710	0.381
2.941	3.337	1.453	0.250	0.479	0.540	0.288	−0.063	0.102	8.164	0.082
3.333	4.309	1.647	0.351	0.531	0.706	0.317	−0.059	0.119	10.757	−0.274
4.167	6.776	2.058	0.615	0.631	1.134	0.371	−0.050	0.156	17.584	−1.297
5.0	9.791	2.470	0.948	0.720	1.666	0.416	−0.040	0.195	26.256	−2.640
6.25	15.243	3.088	1.582	0.884	2.661	0.469	−0.028	0.255	42.815	−5.178
8.333	27.335	4.117	3.003	0.986	4.851	0.529	−0.010	0.360	80.065	−10.527
10.0	39.400	4.940	4.473	1.078	7.083	0.555	0.002	0.446	118.67	−15.597
12.5	61.601	6.175	7.234	1.178	11.234	0.567	0.017	0.576	191.29	−24.238
16.667	109.57	8.234	13.327	1.267	20.299	0.531	0.037	0.797	351.74	−40.711
20	157.82	9.880	19.544	1.288	29.481	0.467	0.049	0.974	515.56	−55.222
25	246.64	12.351	31.109	1.246	46.474	0.317	0.065	1.241	820.39	−78.973
40	631.51	19.761	81.936	0.792	120.61	−0.364	0.096	2.046	2,160.7	−158.85
100	3,947.3	49.402	526.55	−5.007	764.21	−5.802	0.168	5.264	13,887	−583.75
∞	∞	∞	∞	−∞	∞	−∞	∞	∞	∞	−∞

for low-amplitude oscillation, the intersections of this line and the stability curve give the critical flutter speeds. Since the structural damping generally increases with amplitude, the height of the curve above the true damping line is a measure of the violence of flutter; where this height is negative, its magnitude can be interpreted as a "margin of stability."

The use and interpretation of the stability curve depend upon a proper choice of the variable g_i; the one selected should be that most effective in preventing the mode of flutter under investigation. When there are several possible modes, it may be advisable to choose a different variable g for each mode. For instance, there are two common flutter modes in wings, one having a much lower frequency than the other. In the low-frequency mode the damping term in bending has the largest stabilizing effect, while in the high-frequency mode torsional damping is generally most effective. Hence, in this case it is convenient to solve for g_2 (bending) for the larger values of X, and g_1 (torsion) for the smaller values. The two curves may have an overlapping flutter range.

If Eq. (1) were solved for any M_{ii} and only the real parts of each side retained, g_i would be eliminated and an equation in X of degree $2N - 1$ would result, where N is the number of diagonal terms containing X.

TABLE 6

Two-Dimensional Aerodynamic Coefficients, $c = 0.4$

$1/k$	$R_{a\beta}$	$I_{a\beta}$	$R_{b\alpha}$	$I_{b\alpha}$	$R_{b\beta}$	$I_{b\beta}$	R_{bh}	I_{bh}	$R_{c\beta}$	$I_{c\beta}$
0	−0.055	0	−0.055	0	−0.01107	0	−0.062	0	−0.062	0
0.5	0.048	0.208	−0.049	0.062	0.00015	0.036	−0.061	0.009	0.123	0.246
0.833	0.229	0.346	−0.039	0.103	0.02030	0.059	−0.060	0.016	0.464	0.369
1.25	0.584	0.520	−0.018	0.152	0.06023	0.088	−0.057	0.025	1.160	0.449
1.667	1.080	0.693	+0.012	0.199	0.11703	0.114	−0.054	0.035	2.186	0.436
2.0	1.579	0.831	0.042	0.235	0.175	0.134	−0.052	0.043	3.261	0.354
2.5	2.498	1.039	0.101	0.286	0.283	0.161	−0.048	0.056	5.323	0.113
2.941	3.476	1.223	0.165	0.329	0.400	0.183	−0.044	0.068	7.609	−0.216
3.333	4.484	1.386	0.233	0.364	0.521	0.202	−0.041	0.080	10.025	−0.593
4.167	7.036	1.732	0.410	0.434	0.833	0.236	−0.034	0.105	16.392	−1.647
5.0	10.156	2.078	0.633	0.496	1.219	0.264	−0.028	0.131	24.485	−3.003
6.25	15.900	2.598	1.059	0.576	1.941	0.298	−0.020	0.171	39.946	−5.530
8.333	28.309	3.464	2.013	0.682	3.526	0.337	−0.00840	0.242	74.746	−10.795
10.0	40.789	4.157	2.999	0.748	5.139	0.354	−0.00042	0.299	110.82	−15.748
12.5	63.764	5.196	4.852	0.821	8.134	0.362	0.00972	0.387	178.70	−24.152
16.667	113.41	6.928	8.942	0.891	14.666	0.340	0.02308	0.535	328.69	−40.100
20	163.33	8.314	13.114	0.914	21.277	0.301	0.03148	0.654	481.85	−54.108
25	255.23	10.392	20.875	0.897	33.503	0.208	0.042	0.833	766.86	−76.978
40	653.45	16.628	54.989	0.630	86.805	−0.216	0.063	1.373	2,020.0	−153.64
100	4,084.3	41.569	353.389	−3.105	549.06	−3.677	0.111	5.533	12,985	−558.62
∞	∞	∞	∞	−∞	∞	−∞	∞	∞	∞	−∞

TABLE 7

Two-Dimensional Aerodynamic Coefficients, $c = 0.5$

$1/k$	$R_{a\beta}$	$I_{a\beta}$	$R_{b\alpha}$	$I_{b\alpha}$	$R_{b\beta}$	$I_{b\beta}$	R_{bh}	I_{bh}	$R_{c\beta}$	$I_{c\beta}$
0	−0.036	0	−0.036	0	−0.00539	0	−0.04008	0	−0.040	0
0.5	0.068	0.167	−0.032	0.040	0.00246	0.021	−0.03943	0.00575	0.128	0.186
0.833	0.251	0.278	−0.026	0.066	0.01655	0.035	−0.03844	0.00994	0.438	0.271
1.25	0.610	0.417	−0.013	0.098	0.04440	0.051	−0.03681	0.01557	1.075	0.309
1.667	1.113	0.556	+0.005	0.128	0.084	0.067	−0.03491	0.02174	2.013	0.259
2.0	1.618	0.667	0.025	0.151	0.124	0.078	−0.03330	0.02610	2.998	0.151
2.5	2.549	0.833	0.061	0.184	0.199	0.094	−0.03080	0.03515	4.888	−0.121
2.941	3.541	0.980	0.102	0.212	0.280	0.107	−0.02859	0.04279	6.987	−0.469
3.333	4.559	1.111	0.144	0.235	0.364	0.118	−0.02664	0.04986	9.207	−0.858
4.167	7.143	1.389	0.255	0.280	0.578	0.138	−0.02262	0.066	15.059	−1.919
5.0	10.302	1.667	0.395	0.320	0.843	0.154	−0.01887	0.082	22.505	−3.261
6.25	16.116	2.083	0.661	0.373	1.340	0.174	−0.01370	0.107	36.737	−5.732
8.333	28.679	2.778	1.258	0.441	2.424	0.197	−0.00631	0.151	68.783	−10.827
10.0	41.314	3.333	1.875	0.489	3.526	0.207	−0.00131	0.187	102.01	−15.591
12.5	64.573	4.167	3.034	0.540	5.571	0.212	+0.00503	0.242	164.55	−23.635
16.667	114.82	5.555	5.593	0.592	10.023	0.200	0.01339	0.335	302.76	−38.838
20	165.36	6.666	8.204	0.613	14.524	0.178	0.01864	0.409	443.90	−52.153
25	258.40	8.333	13.059	0.613	22.842	0.115	0.02517	0.521	706.56	−73.838
40	661.56	13.333	34.405	0.476	59.078	−0.117	0.03840	0.859	1861.5	−146.33
100	4,135.0	33.332	221.114	−1.743	373.01	−2.105	0.06837	2.210	11,968.0	−526.91
∞	∞	∞	∞	−∞	∞	−∞	∞	∞	∞	−∞

Hence, for a given value of k_0 there is always an odd number of real solutions for X, but never more than $2N - 1$. Some of these solutions may be negative and, hence, of no physical significance. Others may have large negative g_i values; these solutions are of no practical importance because they correspond to conditions of motion under large mechanical driving forces.

In cases of three or more degrees of freedom it is generally unnecessary, therefore, to examine all the roots of Eq. (1). In most cases it is possible from physical considerations and past experience to determine roughly the frequency and speed ranges that are most susceptible to flutter. The corresponding ranges of k_0 and X can then be examined by the methods to be described. Thus, all those solutions that are unimportant from a flutter standpoint are easily eliminated.

SOLUTION OF THE DETERMINANT

A convenient method of solving the determinant is that of successive reduction in order, modified from Frazer, Duncan, and Collar.[7] The scheme is as follows:

(1) Choose the unknown element.

(2) Substitute a trial value of X in all elements except the unknown.

TABLE 8

Two-Dimensional Aerodynamic Coefficients, $c = 0.6$

$1/k$	$R_{a\beta}$	$I_{a\beta}$	$R_{b\alpha}$	$I_{b\alpha}$	$R_{b\beta}$	$I_{b\beta}$	R_{bh}	I_{bh}	$R_{c\beta}$	$I_{c\beta}$
0	−0.021	0	−0.021	0	−0.002	0	−0.02322	0	−0.023	0
0.5	0.081	0.126	−0.019	0.023	0.003	0.011	−0.02285	0.00326	0.126	0.132
0.833	0.262	0.209	−0.016	0.038	0.012	0.018	−0.02229	0.00562	0.403	0.183
1.25	0.615	0.314	−0.008	0.057	0.030	0.027	−0.02137	0.00881	0.972	0.184
1.667	1.111	0.418	+0.002	0.074	0.055	0.034	−0.02030	0.01227	1.813	0.104
2.0	1.609	0.502	0.013	0.088	0.081	0.040	−0.01939	0.01522	2.696	−0.022
2.5	2.525	0.628	0.034	0.107	0.129	0.049	−0.01797	0.01988	4.395	−0.313
2.941	3.503	0.738	0.056	0.123	0.181	0.055	−0.01672	0.02421	6.282	−0.668
3.333	4.506	0.837	0.080	0.137	0.234	0.061	−0.01562	0.02820	8.280	−1.056
4.167	7.052	1.046	0.143	0.163	0.371	0.071	−0.01335	0.03704	13.550	−2.096
5.0	10.164	1.255	0.222	0.187	0.540	0.080	−0.01123	0.04630	20.260	−3.391
6.25	15.895	1.569	0.373	0.218	0.853	0.090	−0.00831	0.061	33.091	−5.750
8.333	28.273	2.092	0.710	0.261	1.539	0.102	−0.00413	0.086	61.997	−10.570
10.0	40.723	2.510	1.059	0.288	2.234	0.107	−0.00130	0.106	91.979	−15.048
12.5	63.642	3.138	1.714	0.319	3.522	0.110	0.00228	0.137	148.42	−22.581
16.667	113.16	4.184	3.161	0.354	6.323	0.104	0.00701	0.189	273.17	−36.760
20	162.96	5.021	4.637	0.369	9.152	0.093	0.00998	0.231	400.58	−49.146
25	254.63	6.276	7.382	0.375	14.376	0.066	0.01367	0.295	637.70	−69.274
40	651.88	10.042	19.449	0.314	37.110	−0.057	0.02115	0.486	1,680.4	−136.37
100	4,074.4	25.104	125.00	−0.872	233.87	−1.069	0.03809	1.250	10,803	−486.55
∞	∞	∞	∞	−∞	∞	−∞	∞	∞	∞	−∞

(3) Read off the magnitudes and angles of these elements from aerodynamic curves.

(4) Star an element in a different row and column from the unknown; the subsequent work is simplified if the starred element does not contain X and if it is a comparatively large element.

(5) Determine the new elements of the determinant of next lower order as illustrated below.

(6) Repeat steps (4) and (5) until the determinant is reduced to second order.

The following third-order determinant is given as an example of this method. Here the element $A_{11} + M_{11}$, or V_{11}, is taken as the unknown, and V_{23} is starred. Each element $A_{ij} + M_{ij}$ is written as a single vector V_{ij}.

$$\begin{vmatrix} V_{11} & V_{12} & V_{13} \\ V_{21} & V_{22} & V_{23}^* \\ V_{31} & V_{32} & V_{33} \end{vmatrix} = 0$$

Reduction to second order is as follows:

$$\begin{vmatrix} V_{11} - \dfrac{V_{13}V_{21}}{V_{23}} & V_{12} - \dfrac{V_{13}V_{22}}{V_{23}} \\ V_{31} - \dfrac{V_{33}V_{21}}{V_{23}} & V_{32} - \dfrac{V_{33}V_{22}}{V_{23}} \end{vmatrix} = 0 \qquad (5)$$

or

$$\begin{vmatrix} V_{11} - V_P & V_{12}' \\ V_{31}' & V_{32}' \end{vmatrix} = 0 \qquad (6)$$

With V_{11} replaced by $A_{11} + M_{11}$, the second-order determinant may be readily expanded to the form

$$A_{11} + M_{11} - V_P = V_{12}'V_{31}'/V_{32}' = V_P'$$

or

$$-M_{11} = A_{11} - V_P - V_P' \qquad (7)$$

When the vectors $-V_P$ and $-V_P'$ are laid off from the point on the A_{11} curve, the closing vector is M_{11}. From the relationships

$$\begin{aligned} M_{11}\ (\text{real}) &= -m_{11}(1 - \Omega_1 X) \\ M_{11}\ (\text{imaginary}) &= m_{11}\Omega_1 g_1 X \end{aligned} \qquad (8)$$

g_1 and X can then be found.

If the calculated X differs from the assumed value, the above procedure is repeated as a trial-and-error problem until agreement is reached; the damping coefficient corresponding to the final value is determined. If the unknown is chosen as previously discussed, convergence of the solution is usually rapid.

Once X is determined, the true air speed for the given set of conditions may be calculated from the relationship

$$v = b_0\omega_0/k\sqrt{X} \qquad (9)$$

From Eqs. (1) to (4) it may be seen that the only effect upon the determinant of a change in altitude occurs in m_{ij}. Altitude may thus be varied by dividing all mechanical coefficients by ρ/ρ_0.

The application of this scheme is not limited to three degrees of freedom. For higher order determinants, reduction follows the same procedure.

THE CIRCLE METHOD

The reciprocal of any vector $V = R + iI$ is

$$1/V = (R - iI)/(R^2 + I^2)$$

This may be expressed in common coordinates as $x + iy$. Then

$$x = R/(R^2 + I^2), \quad y = -I/(R^2 + I^2)$$

Elimination of R yields

$$x^2 + y^2 + (y/I) = 0 \tag{10}$$

If I is positive, this is the equation of a circle below and tangent to the x-axis at the origin and having a diameter $1/I$. As R varies the vector $1/V$ traverses this circle; its exact position is determined by the fact that its angle is the negative of the angle of V.

The above geometric relationship has a useful application in flutter work. For example, the quantity

$$-1/V_{22} = -1/[A_{22} - m_{22}(1 - \Omega_2 X)]$$

is a vector that, as X varies, traverses the circle whose diameter extends from the origin to the point $+1/I_{22}$ on the imaginary axis. Henceforth, this diameter will be treated as a vector that defines the circle. In addition or multiplication the diameter may then be treated as any other vector.

In the simple problem of binary control-surface flutter expressed by the equation

$$\begin{vmatrix} V_{11} & V_{12} \\ V_{21} & V_{22} \end{vmatrix} = 0$$

where V_{12} and V_{21} do not contain X, if the solution is written in the form

$$-M_{11} = A_{11} - (V_{12}V_{21})/V_{22} \tag{11}$$

the right-hand side can be represented by a circle having a diameter vector drawn from the point A_{11}. The diameter will have a magnitude $|V_{12}V_{21}|/I_{22}$ and a direction $\theta_{12} + \theta_{21} + 90$ deg. The exact point on the circle corresponding to a particular value of V_{22} is defined by a line drawn from A_{11} at an angle of 90 deg. $- \theta_{22}$ to the diameter vector, as in Fig. 3. The point so defined is thus the solution to Eq. (11) and gives the components of M_{11}.

Information of a general nature can be drawn from this circle alone. For example, if the circle does not pass below the real axis, flutter cannot occur for any primitive-frequency ratio at the particular value of $1/k_0$ chosen since no positive g_1 solutions exist.

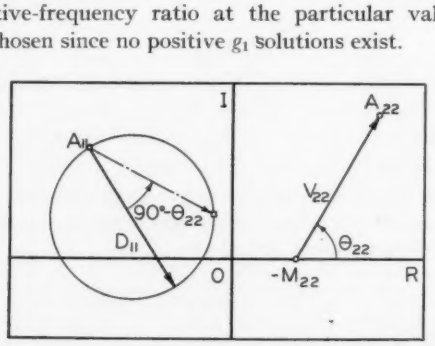

FIG. 3. Stability solution in two degrees of freedom by means of the circle construction.

If either Ω_{22} or m_{22} is uncertain, as for example in a cable-connected control system where cable tension and pilot restraint vary during flight, a conservative solution may be found if only the lower extremity of the circle is used. Eq. (3) applied to M_{11} then determines both X and g_1.

When V_{22} contains a damping term g_2, variations in X cause V_{22} to traverse an oblique instead of a horizontal straight line. The slope of the line is g_2. In this case the diameter vector is rotated through $-\tan^{-1} g_2$, and its magnitude is determined by J_{22} instead of I_{22}, where J_{22} is the perpendicular distance from the origin to the above straight line.

The circle construction is useful in exploring the effects of changes in parameters, particularly when both g_1 and g_2 can be put equal to zero temporarily. Then both the above circle, which is called the (11) circle, and a similar circle (22), obtained by reversing the roles of V_{11} and V_{22} in the above process, can be constructed as shown in Fig. 4. The real axis intersections are values of $-M_{11}$ and $-M_{22}$ which satisfy the determinantal equation. It will be found that the left-hand intersection of the (11) circle combines with right-hand intersection of the (22) circle to form one solution, the other two intersections constituting a second solution. These two solutions are plotted on M_{11} vs. M_{22} coordinates. Curves in this plane are obtained by allowing other parameters, usually k_0 or M_{12}, to vary. The curve shown in Fig. 5 is for constant k_0 and variable M_{12}.

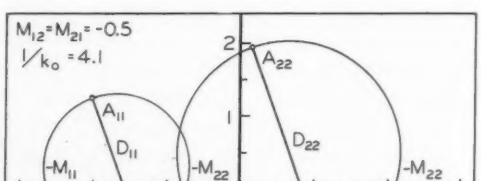

FIG. 4. Two-circle solution used in construction of M-curves.

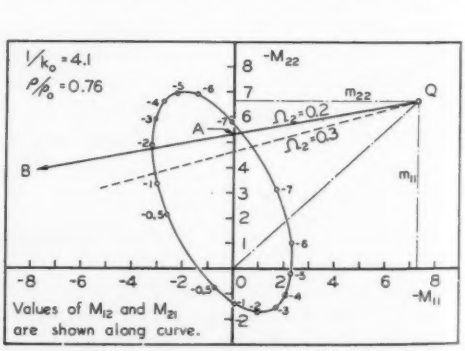

FIG. 5. M-curve as used to study effects of variations in mechanical parameters.

Since both M_{11} and M_{22} are linear in X, combinations that are consistent with Eq. (3) lie along a straight line passing through the point (m_{11}, m_{22}). Intersections of this line, called the pivot line, with the M-curve therefore represent particular solutions to the stability equation. Variations in the primitive-frequency ratio cause the line to pivot about the point (m_{11}, m_{22}). Variations in m_{11} or m_{22} shift the pivot point. Variations in M_{12} or k_0 are shown on the M-curve. The frequency parameter X is a linear function of the distance of the M-curve intersection from the pivot point and is easily determined for all solutions. Hence, for zero structural damping, all possible solutions obtainable by varying the other mechanical parameters can be found. The construction of M-curves is remarkably easy, for when A_{11} and A_{22} are known only the diameter vectors must be calculated.

The application of the M-curve is not necessarily limited to zero structural damping. However, the introduction of a variable g_1 or g_2 usually makes it desirable to restrict one of the other quantities ordinarily allowed to vary.

The circle construction has been found useful in three- and four-degree-of-freedom problems. The method of successive reduction in order described earlier is used, but in this case a diagonal element containing X is starred. Then, if the nondiagonal elements occurring in the same row and column do not contain X, or if they vary slowly with respect to X so that approximate values can be assigned to them, it is clear that the determinant of the next lower order consists of the minor of the starred element but with each aerodynamic term therein replaced by a circle.

In problems of more than two degrees of freedom, for each flutter mode there are usually two degrees of freedom which are more important than the others. If a secondary degree of freedom has a small influence on the total motion because of slight coupling action, the circles obtained by starring the corresponding diagonal element are small and can be treated as perturbations on the vectors that comprise the minor of the starred element. If the influence is small because of a relatively high primitive frequency, the perturbations are given by small arcs of the circles, the angle of arc being determined as in Fig. 3. If the starred element is highly uncertain because of unknown stiffness or inertia parameters, points that, by inspection, appear to represent a condition of least stability may be fixed on the circles; these points are then used to obtain a conservative solution, as in the two-degree-of-freedom case.

Illustrative Example

Analysts who apply the foregoing principles will usually develop personal preferences for particular methods, depending upon their immediate aims and their previous experience. For this reason the preceding discussion has been intended merely as an introduction to many possibilities inherent in graphic methods of stability prediction.

As an illustration of typical steps in the solution of flutter problems, the analysis of a symmetric mode of a twin-fin tail supported rigidly at its plane of symmetry will be outlined.

The coordinates used to describe the motion of the tail are as follows: (1) twist of the stabilizer about the quarter-chord line, the rate of twist being constant and the elevator remaining untwisted; (2) pure stabilizer bending with constant curvature and a node at the plane of symmetry, the outboard vertical surfaces being undeformed; and (3) elevator flapping. As defined by the equation[1]

$$f_i = h_i + \alpha_i x/b_0 + \beta_i r/b_0$$

the weighting factors are

$$\left.\begin{array}{l} h_1 = 0, \quad \alpha_1 = y/S, \quad \beta_1 = -y/S \\ \alpha_2 = \beta_2 = 0,\ h_2 = (y/S)^2 \text{ over the horizontal surface} \\ \alpha_2 = \beta_2 = 0,\ h_2 = 2z/S \text{ over the vertical surfaces} \\ \alpha_3 = h_3 = 0,\ \beta_3 = 1 \text{ over the elevator span} \end{array}\right\} \tag{12}$$

where y is the horizontal surface spanwise station, z is the vertical surface spanwise station measured from the plane of the stabilizer, and S, the reference span, is arbitrarily chosen as the distance from the plane of symmetry to the plane of the vertical fin. For the reference half-chord, b_0, the stabilizer half-chord at the fin-stabilizer intersection is used.

The following weighting factors are introduced for the calculation of aerodynamic coefficients:

$$\left.\begin{array}{l} \alpha_1' = (b/b_0)^2(y/S) \quad \beta_1' = -(b/b_0)^2(y/S) \\ h_2' = (b/b_0)(y/S)^2 \text{ over the horizontal surface} \\ \quad = (b/b_0)(2z/S) \text{ over the vertical surfaces} \\ \beta_3' = (b/b_0)^2 \text{ over the elevator span} \end{array}\right\} \tag{13}$$

These are shown as solid curves in Fig. 6. The broken curves represent reasonable values of the double-primed weighting factors[1] and take into consideration the spanwise pressure effects resulting from departure of the airflow from that of the simple two-dimensional theory applied to each element of span; because of this aerodynamic interaction; the factors extend over both the horizontal and vertical surfaces.

The three-dimensional aerodynamic coefficients are now obtained from Eq. (2).

$$\left.\begin{array}{l} A_{11} = \Sigma[\alpha_1'\alpha_1''A_{a\alpha} + \alpha_1'\beta_1''A_{a\beta} + \beta_1'\alpha_1''A_{b\alpha} + \\ \qquad \beta_1'\beta_1''A_{b\beta}](\Delta y/S) \\ A_{12} = \Sigma[\alpha_1'h_2''A_{ah} + \beta_1'h_2''A_{bh}](\Delta y/S) \\ A_{13} = \Sigma[\alpha_1'\beta_3''A_{a\beta} + \beta_1'\beta_3''A_{b\beta}](\Delta y/S) \\ A_{21} = \Sigma[h_2'\alpha_1''A_{c\alpha} + h_2'\beta_1''A_{c\beta}](\Delta y/S) \\ A_{22} = \Sigma[h_2'h_2''A_{ch}](\Delta y/S) \\ A_{23} = \Sigma[h_2'\beta_3''A_{c\beta}](\Delta y/S) \\ A_{31} = \Sigma[\beta_3'\alpha_1''A_{b\alpha} + \beta_3'\beta_1''A_{b\beta}](\Delta y/S) \\ A_{32} = \Sigma[\beta_3'h_2''A_{bh}](\Delta y/S) \\ A_{33} = \Sigma[\beta_3'\beta_3''A_{b\beta}](\Delta y/S) \end{array}\right\} \tag{14}$$

TABLE 9

Calculation of A_{23} for $1/k_0 = 2.80$, $c = 0.4$

y/S	b/b_0	$1/k_0$	$R_{c\beta}$	$I_{c\beta}$	$\Delta y/S$	h_2'	β_3''	R_{23}	I_{23}
0	1.394	2.00	3.26	0.354	0.0472	0	1.943	0	0
0.094	1.393	2.00	3.26	0.354	0.0945	0.009	1.940	0.005	0.001
0.189	1.363	2.05	3.47	0.330	0.0945	0.049	1.860	0.030	0.003
0.283	1.322	2.11	3.68	0.307	0.0945	0.106	1.750	0.065	0.005
0.378	1.281	2.18	4.00	0.268	0.0945	0.183	1.639	0.113	0.008
0.472	1.242	2.25	4.28	0.239	0.0945	0.276	1.542	0.172	0.010
0.567	1.200	2.32	4.56	0.207	0.0945	0.386	1.444	0.241	0.011
0.661	1.160	2.40	4.90	0.167	0.0945	0.508	1.347	0.316	0.011
0.756	1.119	2.49	5.28	0.122	0.0945	0.640	1.185	0.378	0.009
0.850	1.080	2.58	5.74	0.058	0.0945	0.780	1.010	0.427	0.004
0.945	1.039	2.69	6.24	−0.009	0.0945	0.927	0.825	0.451	−0.001
1.040	0.972	2.87	7.20	−0.157	0.0945	1.050			
1.133	0.648	4.30	17.6	−1.83	0.0945	0.802			
z/S									
−0.154	0.411	6.78	47.8	−6.72	0.0236	0.010	−0.039	0	0
−0.094	0.972	2.87	7.20	−0.157	0.0945	0.009	−0.175	−0.001	0
0	1.162	2.39	4.86	0.172	0.0945	0	±0.390	0	0
0.094	1.151	2.42	4.99	0.157	0.0945	0.010	0.301	0.001	0
0.189	1.024	2.73	6.49	−0.049	0.0945	0.037	0.223	0.005	0
0.283	0.802	3.48	11.14	−0.76	0.0945	0.064	0.146	0.010	−0.001
0.378	0.440	6.35	41.6	−5.74	0.0866	0.063	0.049	0.011	−0.002
							Σ	2.224	0.058

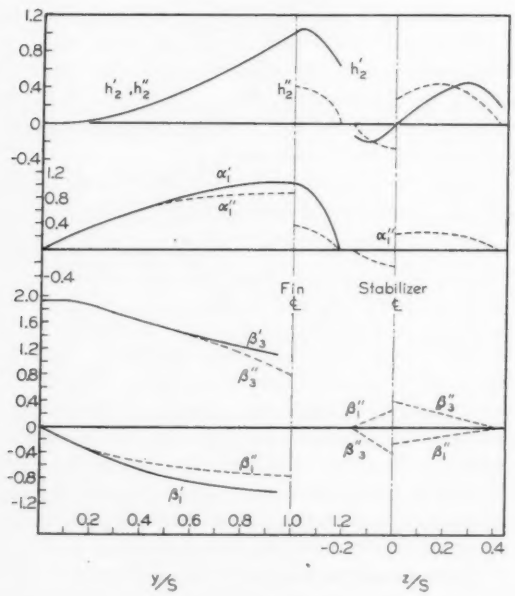

FIG. 6. Variation of aerodynamic weighting factors over the span of the horizontal and vertical surfaces of a twin-fin tail.

The summations extend over both the horizontal and vertical surfaces. As an example, the calculation of A_{23} for a single value of $1/k_0$ is shown in Table 9. Attention is called to the fact that $A_{c\beta}$ varies along the span as a result of the taper; also, the aerodynamic coupling between stabilizer bending and elevator flapping is increased by the aerodynamic forces acting on the vertical surfaces. The rudders, having a high natural frequency for symmetric motion and being fully mass-balanced, are assumed to be rigid parts of the vertical surfaces.

The application of Eq. (4) to the calculation of the inertial parameters is straightforward. For example,

$$m_{11} = \frac{1}{\pi\rho b_0^2 S}\sum\left[\frac{x_0^2 + r_0^2}{b_0^2}\alpha_1^2\,\Delta m + \left(\frac{c_1 x_\beta + r_\beta^2}{b_0^2}2\alpha_1\beta_1 + \frac{r_\beta^2}{b_0^2}\beta_1^2\right)\Delta m_\beta\right] \quad (15)$$

$$m_{22} = \frac{1}{\pi\rho b_0^2 S}\Sigma\,[h_2^2\,\Delta m]$$

In the evaluation of these summations, both the horizontal and vertical spans are usually divided into segments and the individual quantities computed for each segment. Sometimes the vertical surface can be treated as a single unit; in the calculation of m_{11}, the moment of inertia of the vertical surface about a lateral axis can be entered as a single item of the first term. In the calculation of m_{22} the vertical surface appears twice—first, as a single item of weight in the summation over the stabilizer span and, second, in the summation over the vertical span. The latter sum, according to the assumed deflection mode, is $4/S^2$ times the moment of inertia of the vertical surface about a fore-and-aft axis through the stabilizer-fin intersection.

The calculation of the A's and m's constitutes a considerable proportion of the labor involved in any flutter problem. However, convenient tabular forms can be devised by means of which this work can be assigned to computers.

Primitive frequency calculations are carried out without difficulty according to Eqs. (18) and (19) of reference 1. In the present example the determination

of Ω_{12} is particularly simple because the uniformity of the stabilizer structure and the absence of cutouts make it possible to use the equation

$$\Omega_{12} = \Omega_2 x_e/x_0$$

where the elastic axis position x_e and the center of gravity position x_0 are determined in the vicinity of the fin station. By definition, Ω_{ij} is proportional to the work done by the system of forces $F_j \Delta m$ (real) during a virtual displacement equal to f_i. Since the system of forces required to deflect the elevator in mode (3) alone does no work under a virtual displacement in either mode (1) or (2), the remaining structural coupling terms Ω_{13} and Ω_{23} are zero.

When all the mechanical parameters are inserted, the stability equation for standard atmospheric conditions at sea level becomes

$$\begin{vmatrix} A_{11}-5.51[1-X(1+ig_1)] & A_{12}-2.41(1-0.04X) & A_{13}-0.060 \\ A_{21}-2.41(1-0.04X) & A_{22}-5.06(1-0.20X) & A_{23}-0.024 \\ A_{31}-0.060 & A_{32}-0.024 & A_{33}-0.117(1-0.50X) \end{vmatrix} = 0 \tag{16}$$

These coefficients have been calculated for an elevator that is 33 per cent statically balanced, the balance weights being distributed over the outboard third of the elevator span. The torsional frequency is taken as the reference frequency ω_0. The elevator frequency parameter is assumed to be 0.5.

In the solution of this equation by the circle method, it is convenient to star the element V_{33} and reduce the determinant to second order as outlined previously. The circles for each of the four reduced elements are then drawn (Fig. 7). Since the aerodynamic coefficients vary with $1/k_0$ and the mechanical coefficients vary with the density ratio, there is a different circle diagram for each combination of these parameters.

For illustrative purposes, the case of $1/k_0 = 2.80$ and $\rho/\rho_0 = 0.58$ may be considered. The determinant is then that of Eq. (16) with all the mechanical parameters divided by 0.58. Through use of a scale and protractor, the following vector magnitudes and directions are determined as shown in Fig. 2: $V_{31} = 0.243$, 150 deg.; $V_{13} = 1.68$, 24 deg.; $V_{32} = 0.067$, 160 deg.; $V_{23} = 2.18$, 1 deg. The imaginary part of V_{33} is found to be 0.331. The magnitudes and directions of the diameter vectors are

$$D_{11} = \frac{|V_{13}\, V_{31}|}{I_{33}} = 1.23 \qquad \theta_{13} + \theta_{31} + 90\,\text{deg.} = 264\,\text{deg.}$$

$$D_{12} = \frac{|V_{13}\, V_{32}|}{I_{33}} = 0.342 \qquad \theta_{13} + \theta_{32} + 90\,\text{deg.} = 274\,\text{deg.}$$

$$D_{21} = \frac{|V_{23}\, V_{31}|}{I_{33}} = 1.60 \qquad \theta_{23} + \theta_{31} + 90\,\text{deg.} = 241\,\text{deg.}$$

$$D_{22} = \frac{|V_{23}\, V_{32}|}{I_{33}} = 0.445 \qquad \theta_{23} + \theta_{32} + 90\,\text{deg.} = 251\,\text{deg.}$$

The diameters are laid off from the respective points A_{11}, A_{12}, A_{21}, and A_{22}, and the four circles are constructed.

The particular arrangement of Fig. 7, with the circles drawn on two vertically aligned sets of axes, is useful in finding consistent sets of values for the mechanical terms M_{11}, M_{12}, M_{21}, and M_{22}. All of these coefficients are linear functions of X. With $-M_{11}$ on the upper horizontal axis and $-M_{12}$ $(= -M_{21})$ on the lower horizontal axis, linearity requires that corresponding values of the two coefficients always be on a straight line passing through a fixed point P_1. Similarly, $-M_{22}$ and $-M_{21}$ must lie on a straight line pivoting about a point P_2. The two pivots are easily located by drawing the lines for any two values of X. For any value of $-M_{11}$, the corresponding value of $-M_{12}$ $(= -M_{21})$ is then given by the intersection with the lower axis of the line connecting the points $-M_{11}$ and P_1, and $-M_{22}$ is given by the intersection with the upper axis of the line through the points P_2 and $-M_{12}$.

In the event that M_{12} and M_{21} are independent of X, the circle diagram may be further simplified. The (11) circle is drawn on the upper plot; the (22) circle, on the lower one; $-M_{11}$ and $-M_{22}$ then require but a single pivot point. The other two circles may be placed wherever convenient.

To return to the solution itself, it may be seen that corresponding points on the four circles are determined by the angle of V_{33}, as in Fig. 3. These points are the termini of the vectors $\overline{V}_{11}$, $\overline{V}_{12}$, $\overline{V}_{21}$, and $\overline{V}_{22}$, the elements of the reduced determinant, drawn from the respective $-M$ points. If now

$$\overline{V}_{11}\overline{V}_{22} = \overline{V}_{12}\overline{V}_{21} \tag{17}$$

the determinantal equation is satisfied. But since the imaginary part of $-M_{11}$ is unknown, it is convenient to draw $\overline{V}_{11}$ from the point $-M_{11}$ (real) to the vertical line through the point on the (11) circle; the length d (Fig. 7) then is $-M_{11}$ (imaginary).

As a first trial in the solution under consideration, it is assumed that $-M_{11}$ (real) $= 0$. This value corre-

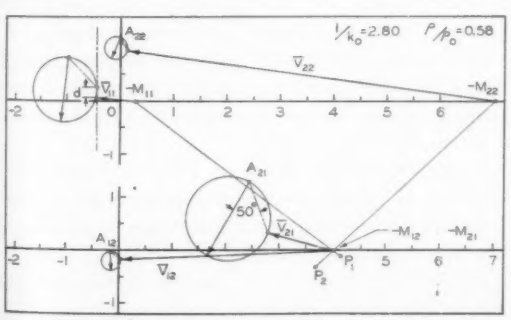

FIG. 7. Circle diagram, showing solution of the vector equation in three degrees of freedom.

sponds to an X of unity, for which condition θ_{33} is found to be 40 deg. The other three M's are determined by means of the pivot point relationships, the points on the circles are located at an angle 90 deg. $-\ \theta_{33} = 50$ deg. to the diameters, and the following vectors are measured: $\overline{V}_{12} = 3.98$, 182 deg.; $\overline{V}_{21} = 1.26$, 165 deg.; $\overline{V}_{22} = 6.90$, 172 deg. From Eq. (17), $\overline{V}_{11}$ is found to be 0.73, 175 deg.

The calculated $\overline{V}_{11}$, when drawn from the real axis so that its terminus falls on the vertical line $R = -0.44$ drawn through the point on the (11) circle, determines a new point $-M_{11}$ (real) $= 0.29$. When the trial solution is repeated with this assumption, $\overline{V}_{12}$ and $\overline{V}_{21}$ show practically no change; $\overline{V}_{22}$ and $\overline{V}_{11}$ become 6.95, 172 deg., and 0.72, 175 deg., respectively; and $-M_{11}$ (real) retains the above value. The quantities X and g_1 are calculated from Eq. (3) as follows:

$$X = \frac{m_{11} + M_{11}\,(\text{real})}{m_{11}\Omega_1} = \frac{9.51 - 0.29}{(9.51)(1)} = 0.97$$

$$g_1 = \frac{d}{m_{11} + M_{11}\,(\text{real})} = \frac{-0.21}{9.51 - 0.29} = -0.023$$

This value of X does not appreciably shift the points on the circles as originally located for $X = 1.0$.

With the same determinant and the same set of circles, it is often possible to find additional solutions corresponding to other values of X. The various solutions can then be approximately examined in order to determine the most critical flutter mode.

The solutions obtained by varying $1/k_0$ and ρ/ρ_0 are conveniently plotted as shown in Fig. 8. Only one flutter mode is represented, since the others are less critical in this case. The horizontal scale, $1/k_0\sqrt{X}$, becomes true air speed when multiplied by the reference speed $v_0 = b_0\omega_0$. Critical speeds for various altitudes are determined by the abscissas corresponding to an estimated or experimentally determined value of the structural damping factor g_1.

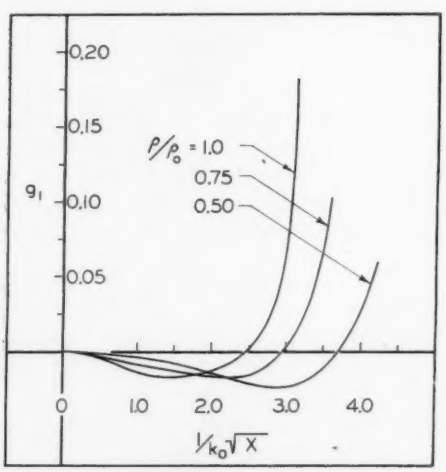

FIG. 8. Stability curves showing critical speed factors for various altitudes and damping factors.

It will, of course, be understood that high accuracy cannot be obtained by the above process. However, many parameters are usually so uncertain that an extremely precise solution is not warranted. If greater accuracy is desired, it can be obtained with little extra work by direct substitution of the graphically determined X in the stability equation.

The flutter characteristics determined from the stability curve indicate the limits of safe operation for the airplane under consideration. If these limits restrict performance too greatly, a survey is made to determine the design changes that will improve the airplane most efficiently.

The effects of variations in elevator parameters are readily observed in the circle diagram, Fig. 7. Changes in elevator frequency or moment of inertia merely shift the points on the four circles, while changes in balance alter the diameter vectors. In this case, however, the elevator parameters are found to have little influence on the critical flutter speeds.

For the study of variations in other mechanical parameters it is convenient to make Ω_3 infinite and thereby reduce the problem to one of two degrees of freedom. Suppression of the elevator flapping mode is permissible here because of its ineffectiveness in promoting flutter. Now the M-curve for zero damping may be constructed as explained earlier; the sample solution of Fig. 4 and the plot of Fig. 5 are actual applications from the subject problem.

The closed curve (Fig. 5) is shown for $1/k_0 = 4.1$, a value that is critical for this problem. As an example of the use of the curve, pivot lines are shown for $\Omega_2 = 0.2$ and $\Omega_2 = 0.3$, both drawn for $\rho/\rho_0 = 0.76$. The intersections of these lines with the curve determine values of M_{12} for which the stability curves have axis intercepts at $1/k_0 = 4.1$. From the shape of these latter curves critical speeds can be estimated for particular damping factors when the intercepts are known.

From the figure it is clear that for $\Omega_2 = 0.2$ the stabilizer unbalance term $-M_{12}$ must be reduced from 3.2 to 1.8 in order to shift the intercept above $1/k_0 = 4.1$, while for $\Omega_2 = 0.3$ a reduction from 3.2 to 1.2 is required. The same result would be accomplished by an increase in m_{22} from 6.7 to 8.1 in the first case and from 6.7 to 9.0 in the second, since these changes would translate the line $\overline{QB}$ upward until it intersects the curve at $-M_{12} = 3.2$.

Through use of the M-curve, then, the effects of any changes in structure or mass distribution can be readily estimated. For example, added mass along the stabilizer leading edge would have two important beneficial effects—a reduction in $-M_{12}$ and an increase in m_{22}—and one minor adverse effect—an increase in m_{11}.

The fact that the curve is a closed loop shows that large values of $-M_{12}$, as well as small values, are bene-

ficial provided they can be attained without adverse effects on the other parameters.

Conclusion

The type of information desired and the nature of the data available vary so widely from one flutter problem to another that the methods used must be extremely flexible in order to be generally applicable. Detailed procedures making use of the general ideas presented here will occur to the analyst as the need arises in particular problems.

The primary assumptions upon which any problem is based are determined by: the nature and accuracy of available data; the importance of an accurate solution from the standpoint of safety, performance, and manufacturing costs; the status of the problem in relation to future designs; the complexity of three-dimensional aerodynamic and mechanical effects; and the time and man power available. Six degrees of approximation are recognized: (1) substitution for the actual system of a two-dimensional setup having the properties of a particular section of the airfoil—for example, the three-quarter span station of a wing; (2) the same, except that some or all of the mechanical parameters are calculated in three dimensions; (3) calculation of both aerodynamic and mechanical parameters in three dimensions with the assumption of no taper or spanwise aerodynamic interaction; (4) the same, except that interspan effects such as the tip vortex and interaction between horizontal and vertical surfaces are considered qualitatively; (5) complete three-dimensional problem except that interspan effects are neglected; (6) inclusion of all known three-dimensional effects.

Most problems involving small, moderate-speed aircraft can be treated two-dimensionally by approximations (1) and (2). The extensive work of Wylie[8, 9, 10] makes it unnecessary to do more than determine the equivalent two-dimensional mechanical parameters, except in cases of more than two degrees of freedom or in problems involving tabs. In approximation (3) the two-dimensional aerodynamic coefficients appear in different ratios than those in Wylie's work, and his solutions cannot be used.

For flutter problems that do not readily yield to the simplifying assumptions, such as those involving the complex modes on extremely large airplanes, one of the approximations—(4), (5), or (6)—is used. The fact that these solutions generally can be applied qualitatively to other designs besides the specific model under investigation is justification for extended computation. It is to be expected that, as such problems are solved in detail, short cuts will appear along with a better understanding of the relative importance of different parameters and that this knowledge can be applied to advantage in subsequent analyses.

In modern high-speed aircraft the effects of compressibility must be considered. Possio[11] has shown that in the case of an oscillating wing compressibility causes large changes in the aerodynamic coefficients, the effects being functions of both speed and frequency. In addition, when local speeds exceed the speed of sound, the shock fronts and accompanying burbles introduce nonlinear effects that can best be studied experimentally. The existence of these complex aerodynamic effects at extremely high speeds and our limited knowledge of three-dimensional airflow make it necessary occasionally to supplement theoretic results with wind-tunnel tests and flight experience.

References

[1] Bleakney, W. M., *Three-Dimensional Flutter Analysis*, Journal of the Aeronautical Sciences, Vol. 9, No. 2, pp. 56–63, December, 1941.

[2] Kassner, R., and Fingado, H., *Das Ebene Problem der Flugelschwingung*, Luftfahrtforschung, Vol. 13, No. 11, pp. 374–387, November, 1936.

[3] Bergen, W. B., and Arnold, Lee, *Graphical Solution of the Bending-Aileron Case of Flutter*, Journal of the Aeronautical Sciences, Vol. 7, No. 2, pp. 495–508, October, 1940.

[4] Arnold, Lee, *A Vector Solution of the Three-Degree Case of Wing Bending, Wing Torsion, Aileron Flutter*, Institute of the Aeronautical Sciences, Tenth Annual Meeting, New York, January 30, 1942 (to be published).

[5] Theodorsen, Theodore, *General Theory of Aerodynamic Instability and the Mechanism of Flutter*, N.A.C.A. T.R. No. 496, 1935.

[6] Theodorsen, Theodore, and Garrick, I. E., *Mechanism of Flutter, A Theoretical and Experimental Investigation of the Flutter Problem*, N.A.C.A. T.R. No. 685, 1940.

[7] Frazer, R. A., Duncan, W. J., and Collar, A. R., *Elementary Matrices*, Cambridge University Press, 1938.

[8] Aircraft Airworthiness Section Report No. 22, *Flexure-Torsion Binary Flutter*, C.A.A., January, 1941.

[9] Aircraft Airworthiness Section Report No. 23, *Perpendicular Axes Control Surface Binary Flutter*, C.A.A., April, 1941.

[10] Engineering Section Report No. 24, *Parallel Axes Control Surface Binary Flutter*, C.A.A., September, 1941.

[11] Possio, Camillo, *L'Azione Aerodinamica sul Profilo Oscillante in un Fluido Compressible a Velocità Iposonora*, L'Aerotecnica. Vol. 18, No. 4, pp. 441–471, April, 1938.

A Simplified Two-Dimensional Theory of Thin Airfoils

H. J. STEWART*

California Institute of Technology

Introduction

IN THE EXISTING SOLUTIONS of the thin airfoil problem, the determination of the steady state lift and moment of an airfoil of small camber and thickness, as given by Birnbaum,[1] von Kármán,[2] C. B. Millikan,[3] etc.,[4, 5] the velocity potential for the flow is determined, and the lift distribution and the integrated lift and moment are found from this result. It appears that a somewhat simpler solution of this problem can be obtained by working directly with the velocity components rather than with the velocity potential. This same method can also be used to advantage in many three-dimensional wing problems. An important feature of this method is that the inverse problem, the determination of an airfoil shape that will produce a given lift distribution, can be solved just as easily as the direct problem. Both the direct and the inverse problem will be investigated by this method in the present paper.

The notations used in the analysis are as follows:

x, y = rectangular coordinates in the plane of the airfoil
c = chord of airfoil
i = $\sqrt{-1}$
z = $x + iy$
u, v = velocity components in the x and y directions, respectively
w = $u - iv$ = complex velocity
w' = complex velocity due to the airfoil
w'' = complex velocity due to the airfoil camber
U = velocity of air far from the airfoil
α = inclination of the flow far from the airfoil
p = static pressure
Δp = differential in static pressure between the lower and upper surface of the airfoil
ρ = fluid density
q = $\frac{1}{2}\rho U^2$ = dynamic pressure
η = airfoil ordinate
L = $C_L q c$ = lift of airfoil per unit span
M = $C_M q c^2$ = pitching moment about the center of the airfoil per unit span

The fundamental equations for the two-dimensional irrotational motion of an incompressible fluid are

$$\frac{\partial u}{\partial x} = -\frac{\partial v}{\partial y} \tag{1}$$

and

$$\frac{\partial u}{\partial y} = \frac{\partial v}{\partial x} \tag{2}$$

which are the conditions imposed by continuity and irrotationality, respectively. If velocity components are found which satisfy these equations for any given boundary conditions, the pressure distribution for steady state motion may then be calculated from the equation

$$p + \tfrac{1}{2}\rho\,[u^2 + v^2] = \text{constant} \tag{3}$$

which is an integral of the equations of motion. If Eqs. (1) and (2) are considered as Cauchy-Riemann equations, they imply that the complex velocity $w = u - iv$ must be an analytic function of the complex variable $z = x + iy$, or

$$u - iv = w(z) \tag{4}$$

If the airfoil ordinates are given by $\eta(x)$ (Fig. 1), a boundary condition for determining $w(z)$ is that the flow must not cross the surface of the airfoil; that is

$$v = u(\partial\eta/\partial x) \tag{5}$$

on the surface of the airfoil. A second boundary condition is that far from the airfoil the flow must be a rectilinear flow of constant velocity. The third boundary condition, the Kutta condition, is that the velocity must be finite in the neighborhood of the trailing edge. If the airfoil is thin and only slightly cambered, the first boundary condition may be considered as applying along the x axis rather than on the actual airfoil surface.

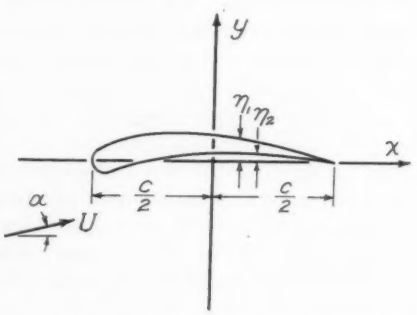

FIG. 1. Sketch showing the notation used in the thin airfoil analysis.

In order to determine $w(z)$, it is convenient to introduce another complex variable $\zeta = re^{i\theta}$ where

$$(4/c)z = \zeta + (1/\zeta) \tag{6}$$

The points for which $r \geqslant 1$ will be considered as those that transform into the z-plane. It is readily seen that

Presented at the Aerodynamics Session, Tenth Annual Meeting, I.Ae.S., New York, January 30, 1942.

* Assistant Professor of Aeronautics and Meteorology.

points on the circle $r = 1$ in the ζ-plane correspond to points on the x axis in the z-plane where

$$x = (c/2) \cos \theta \tag{7}$$

The boundary condition of Eq. (5) may thus be considered as applying on the unit circle in the ζ-plane.

Lift and Moment of the Airfoil

The total lift and pitching moment of the airfoil are most easily calculated by using the Blasius equations. If X and Y are the resultant force components in the x and y directions, respectively, then

$$X - iY = (\rho i/2) \oint w^2 dz \tag{8}$$

where the integration is carried over any contour in the fluid enclosing the airfoil. Similarly, the stalling moment of the airfoil about the origin is

$$M = Rl[(\rho/2) \oint w^2 z dz] \tag{9}$$

The velocity field around any airfoil may be expanded in a series, valid for large values of ζ, of the form

$$w = U \sum_{n=0}^{\infty} (a_n + ib_n) \zeta^{-n} \tag{10}$$

where the a_n's and b_n's are all real, $a_0 + ib_0 = e^{-i\alpha}$ and $a_1 = 0$ since the airfoil is a closed body. From this, the resultant lift and moment are

$$\begin{aligned} L &= (\rho/2) U^2 c \pi b_1 \\ \text{and } M &= (\rho/2) U^2 c^2 \tfrac{\pi}{4} [a_2 \sin \alpha - b_2 \cos \alpha] \end{aligned} \tag{11}$$

Thus, the lift and pitching moment coefficients are

$$\begin{aligned} C_L &= \pi b_1 \\ \text{and } C_M &= \tfrac{\pi}{4} [a_2 \sin \alpha - b_2 \cos \alpha] \end{aligned} \tag{12}$$

If the lift distribution is desired, it may be calculated from Eq. (3) once the velocity field has been determined.

The Flat Plate Airfoil

The suggested method will first be used to solve exactly the problem of the flat plate airfoil. The airfoil is placed on the x-axis with its leading and trailing edges at $x = -c/2$ and $x = c/2$, respectively, as in Fig. 2. If the airfoil is at an angle of attack α, then $w(z)$ can be written as

$$w(z) = Ue^{-i\alpha} + w'(z) \tag{13}$$

where $w' = u' - iv'$ is the velocity due to the airfoil. From Eq. (5), $v = 0$ and, hence, $v' = -U \sin \alpha =$ constant on the airfoil. $w'(z)$ must also satisfy the Kutta condition and vanish as $z \to \infty$. It is easily seen that the function

$$w_0(z) = -[2i/(\zeta + 1)] \tag{14}$$

satisfies the latter two conditions and on the airfoil gives $v_o = 1$. From this, the flow around a flat plate is given by

$$w(z) = Ue^{-i\alpha} + (2iU \sin \alpha)/(\zeta + 1) \tag{15}$$

On the airfoil this gives, of course, no vertical velocity and the horizontal velocity is

$$u = U[\cos \alpha + \sin \alpha \tan (\theta/2)] \tag{16}$$

If the velocity is expanded in a series of the type used in Eq. (10), it is found that for $n \geqslant 1$,

$$a_n + ib_n = -2i \sin \alpha \, (-1)^n \tag{17}$$

The lift and moment coefficients for a flat plate airfoil are thus

$$\begin{aligned} C_L &= 2\pi \sin \alpha \\ C_M &= \frac{\pi}{2} \sin \alpha \cos \alpha \end{aligned} \tag{18}$$

These are both well-known results. The pressure distribution over the plate is given by Eq. (3) as

$$p = -\rho U^2 \{\sin \alpha \cos \alpha \tan (\theta/2) - \tfrac{1}{2} \sin^2 \alpha \, [1 - \tan^2(\theta/2)]\} \tag{19}$$

where the pressure has been taken as zero far from the airfoil.

The Airfoil of Zero Thickness

Airfoils having zero thickness and a small camber will next be investigated. The leading and trailing edges are again placed at $x = \pm c/2$ as in Fig. 3. It will be assumed that both the camber $\eta(x)$ and the angle of

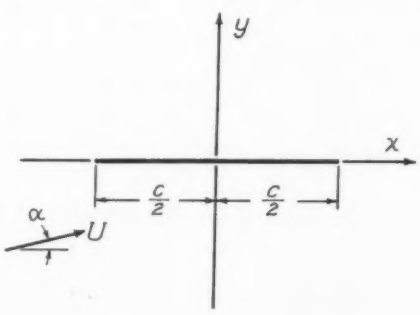

Fig. 2. The flat plate airfoil.

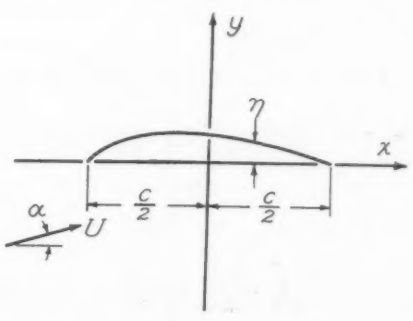

Fig. 3. The cambered airfoil of zero thickness.

attack α are small quantities of the first order. Squares and higher powers of these quantities will be neglected as compared to the first-order terms. With this approximation and in view of Eqs. (14) and (15), the velocity field may be written as

$$w(z) = U(1 - i\alpha) - U\alpha w_0 + w'' \tag{20}$$

where w'' is the velocity due to camber. In the linearized form the boundary condition of Eq. (5) may be written as

$$v'' = U(\partial\eta/\partial x) \tag{21}$$

It can be seen that this linearized boundary condition breaks down in the neighborhood of the leading edge where $x + (c/2)$ is of the order of $c\alpha^2$.

Since the airfoil is of zero thickness, v'' must be an even function of θ, and the most general expression for w'' is

$$w'' = Ui \sum_{n=1}^{\infty} b_n'' \zeta^{-n} \tag{22}$$

This expression automatically satisfies the Kutta condition. This series may not converge on the airfoil, but, if it does, the velocities there are

$$\left.\begin{aligned} u'' &= U \sum_{n=1}^{\infty} b_n'' \sin n \\ \text{and} \qquad & \\ v'' &= -U \sum_{n=1}^{\infty} b_n'' \cos n \end{aligned}\right\} \tag{23}$$

In order to determine the b_n'''s, a cosine expansion for $\partial\eta/\partial x$ must first be obtained. Let

$$\partial\eta/\partial x = c_0/2 + \sum_{n=1}^{\infty} c_n \cos n\theta \tag{24}$$

where

$$c_n = 2/\pi \int_0^{\pi} (\partial\eta/\partial x) \cos n\theta \, d\theta \tag{25}$$

As this series contains in general a constant term, $c_0/2$, the series expansion for w'' will not in general converge on the airfoil; however it is apparent from the results of the analysis of the flat plate airfoil that w'' may be written as

$$w'' = -[Uic_0/(\zeta + 1)] - Ui \sum_{n=1}^{\infty} c_n \zeta^{-n} \tag{26}$$

where the latter series converges on the airfoil. By expanding w'' in a series of the type of Eq. (10), it is found that

$$\begin{aligned} a_n'' + ib_n'' &= i[(-1)^n c_0 - c_n] \\ &= -\frac{2i}{\pi} \int_0^{\pi} \left(\frac{\partial\eta}{\partial x}\right) [\cos n\theta - (-1)^n] d\theta \end{aligned} \tag{27}$$

The coefficients for the term $-U\alpha w_0$ of Eq. (20) must be added to Eq. (27) to obtain the total lift and moment coefficients. These are

$$\begin{aligned} C_L &= 2\pi\alpha - 2\int_0^{\pi} \left(\frac{\partial\eta}{\partial x}\right) (1 + \cos\theta) d\theta \\ C_M &= \frac{\pi}{2}\alpha + {}^1/_2 \int_0^{\pi} \left(\frac{\partial\eta}{\partial x}\right) (\cos 2\theta - 1) d\theta \end{aligned} \tag{28}$$

These results may be stated in a more familiar form if the integrals are transformed by integration by parts. The results are then

$$\begin{aligned} C_L &= 2\pi\alpha + \frac{8}{c^2} \int_{-c/2}^{c/2} \frac{\eta(x)\, dx}{[1 - (2x/c)]\sqrt{1 - (2x/c)^2}} \\ C_M &= \frac{\pi}{2}\alpha - \frac{8}{c^3} \int_{-c/2}^{c/2} \frac{\eta(x) x\, dx}{\sqrt{1 - (2x/c)^2}} \end{aligned} \tag{29}$$

These are the well-known Munk integrals.

The lift distribution can be obtained from Eq. (3). In a linearized form this can be written as

$$p = -\rho U(u - U) \tag{30}$$

where the pressure is taken as zero far from the airfoil. If this result is combined with Eqs. (20) and (26), it is seen that the pressure distribution over the airfoil is given by

$$p = -\rho U^2 \left[\left(\alpha - \frac{c_0}{2}\right) \tan\frac{\theta}{2} - \sum_{n=1}^{\infty} c_n \sin n\theta \right] \tag{31}$$

This expression can be used to calculate hinge moments or, if the lift distribution is given as in the inverse problem, Eq. (31) determines the required camber line.

The Effect of Thickness

The analysis of an airfoil of small but finite thickness, as in Fig. 1, can be carried out in a similar manner. For this purpose it is convenient to consider the airfoil as being built up with a thickness function η_t and a camber function η_c where

$$\begin{aligned} \eta_t &= {}^1/_2(\eta_1 - \eta_2) \\ \text{and } \eta_c &= {}^1/_2(\eta_1 + \eta_2) \end{aligned} \tag{32}$$

With negative values of θ corresponding to the bottom side of the airfoil and positive values to the top, $\partial\eta/\partial x$ may be expanded in the Fourier series

$$\frac{\partial\eta}{\partial x} = \frac{c_0}{2} + \sum_{n=1}^{\infty} c_n \cos n\theta + \sum_{n=1}^{\infty} d_n \sin n\theta \tag{33}$$

where

$$c_n = 2/\pi \int_0^{\pi} (\partial\eta_c/\partial x) \cos n\theta \, d\theta \tag{34}$$

and

$$d_n = 2/\pi \int_0^{\pi} (\partial\eta_t/\partial x) \sin n\theta \, d\theta \tag{35}$$

The flow around the airfoil is then

$$w = U(1 - i\alpha) - \frac{2iU}{\zeta + 1}\left(-\alpha + \frac{c_0}{2}\right) - Ui\sum_{n=1}^{\infty} c_n\zeta^{-n} + U\sum_{n=1}^{\infty} d_n\zeta^{-n} \quad (36)$$

From this, it is apparent that the thickness function has no effect on the lift distribution or lift or moment. These are all determined by the camber function. The lift, moment and lift distribution are thus given by Eqs. (28) and (31) if they are applied to the camber function.

The pressure distribution due to the thickness function is found from the linearized pressure equation to be

$$p = -\rho U^2 \sum_{n=1}^{\infty} d_n \cos n\theta \quad (37)$$

This can be added to the pressure distribution due to the camber, Eq. (31), to obtain the resulting pressure distribution.

Numerical Examples

The results of the analysis will now be applied to several examples.

Example 1

The first problem to be investigated is the determination of the lift, pitching moment and lift distribution of a parabolic arc airfoil (Fig. 4) at zero angle of attack.

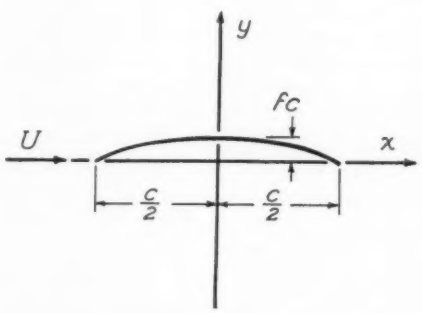

Fig. 4. The parabolic arc airfoil.

For this case

$$\eta = fc[1 - (2x/c)^2] \quad (38)$$

and

$$\partial\eta/\partial x = -2fc(2x/c)(2/c) = -4f\cos\theta \quad (39)$$

From Eqs. (24) and (27),

$$c_1 = -4f \text{ and } b_1'' = 4f \quad (40)$$

All other coefficients are zero. The lift and moment coefficients are

$$C_L = 4f\pi$$
$$C_M = 0 \quad (41)$$

From Eq. (31), the pressure distribution is

$$p = (-\rho U^2)(4f\sin\theta) \quad (42)$$

This shows that the lift is elliptically distributed across the chord.

Example 2

As a second example, a camber function will be calculated which will produce a lift distribution across the chord which is constant for the leading half of the chord and is zero for the trailing half. For this lift distribution the pressure on the rear half of the airfoil is zero, and on the top of the front half it is

$$p = -C_L(\rho/2)U^2 \quad (43)$$

This pressure distribution must be an odd function of the angle θ, and, if it is expanded in a sine series as in Eq. (31), the coefficients are found to be

$$c_n = \frac{C_L}{n\pi}\left\{\cos n\pi - \cos n\frac{\pi}{2}\right\} \quad (44)$$

The slope of the camber function is then

$$\partial\eta/\partial x = \sum_{n=1}^{\infty} c_n \cos n \quad (45)$$

If this is integrated term by term using the condition that $\eta = 0$ at the trailing edge, it is seen

$$\eta = -\frac{c}{4}\left[c_1\frac{1 - \cos 2}{2} + \sum_{n=2}^{\infty} c_n\left(\frac{1 - \cos(n+1)\theta}{n+1} - \frac{1 - \cos(n-1)\theta}{n-1}\right)\right] \quad (46)$$

In this case and in most cases where the pressure distribution is geometrically simple the series may be summed and the camber function may thus be expressed in a closed form. If the coefficients c_n of Eq. (44) are inserted in Eq. (36), it is easily seen that

$$w = U - Ui\frac{C_L}{\pi}\left[\tfrac{1}{2}\log\left(1 + \frac{1}{\zeta^2}\right) - \log\left(1 + \frac{1}{\zeta}\right)\right] \quad (47)$$

On the unit circle where $\zeta = e^{i\theta}$, this becomes

$$w = U - Ui\frac{C_L}{2\pi}\log\frac{\cos\theta}{1 + \cos\theta} \quad (48)$$

and the slope of the camber function is

$$\frac{\partial\eta}{\partial x} = \frac{C_L}{2\pi}\log\frac{|\cos\theta|}{1 + \cos\theta} \quad (49)$$

This can be readily integrated and the camber function is found to be

$$\frac{4\pi\eta}{C_{LC}} = 2 \log 2 + \cos\theta \log |\cos\theta| - (1 + \cos\theta) \log (1 + \cos\theta) \quad (50)$$

This camber function is shown in Fig. 5. It may be noted that the s-curvature of the airfoil is just sufficient so that the pitching moment about the quarter chord point is zero.

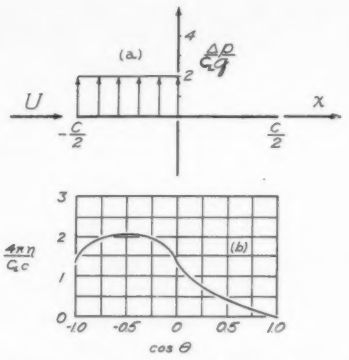

FIG. 5. (a) The lift distribution produced by the camber function (b).

REFERENCES

[1] Birnbaum, W., *Die Tragende Wirbelfläche als Hilfsmittel zur Behandlung des ebenen Problems der Tragflügeltheorie*, ZAMM, Vol. 3, pp. 290, 1923.

[2] Durand, W. F., *Aerodynamic Theory*, Vol. 2, Julius Springer, Berlin, 1934.

[3] Millikan, C. B., *An Extended Theory of Thin Airfoils and Its Application to the Biplane Problem*, N.A.C.A. T.R. No. 362.

[4] Keune, F., *Die ebene Potentialströmung um Allgemeine dicke Tragflügelprofile*, 1938 Yearbook of German Aero. Research, p. I 13.

[5] Gebelein, H., *Verallgemeinerung der Birnbaumschen Theorie für die Potentialströmung um mässig dicke Profile*, 1938 Yearbook of German Aero. Research, p. I 27.

Letter to the Editor

Dear Sir:

In the paper by F. N. M. Brown, "The Space-Time Recorder" (June, 1942, JOURNAL), it is not stated what accuracy the photographic type is capable of except to affirm its superiority to other types which are described as having an inertia error of the order of 0.1 to 0.15 g. One source of error not discussed by the author arises in taking off the displacements from the record. Using 0.1g as a desirable limit of error and $^1/_{240}$ of a second as the time interval, we may calculate the displacement error which is

$$\frac{0.1 \times 32 \times 12}{2 \times 240 \times 240} \text{ in.}$$

This dimension, one-third of one-thousandth of an inch, is further reduced by the scale of the image. In the instrument described by the author the reduction factor is one-tenth to one-half. The probable error in taking the displacements off the record is of the order of at least ten times this magnitude or a corresponding error in the acceleration of 2g.

One obvious cure for this error is to increase the time interval. But this has its limitations since the acceleration calculated is the average over the longer time interval.

As a means of measuring airplane landing stresses, the space-time recorder, along with the accelerometer, is of limited usefulness. Unfortunately, the airplane is not a rigid body and the simultaneous accelerations of its various masses vary widely. Since the total landing force depends on the accelerations of all the masses, we cannot use a single acceleration for its calculation unless we know the shape to which the structure is distorting. The accuracy with which we must know this distortion is indicated by the preceding calculation. From it, it is evident that the assumption that equal accelerations occur at two points in the structure is in error by 0.1g when a relative distortion at the two points of 0.00033 in. occurs in $^1/_{240}$ of a second.

E. S. JENKINS
Chief of Materials and Structures Research
Curtiss-Wright Corporation

A Simple Method of Applying the Compressibility Correction in the Determination of True Air Speed

WM. C. SCHOOLFIELD*
United Aircraft Corporation

SUMMARY

By reviewing the complete impact pressure equation, which describes the pressure exerted by an air stream upon coming to rest, it is shown that the approximating assumption that is involved in the customary method of determining the true air speed of an airplane at altitude is no longer satisfactory for high-speed airplanes. The compressibility error that is a result of this assumption is isolated, and a method is described whereby the necessary correction may be applied by constructing additional altitude curves of indicated air speed ($V\sqrt{\sigma}$) on the conventional air-speed indicator calibration chart. The true air speed at any altitude is then determined by the usual method—from the known value of indicated air speed and atmospheric pressure and temperature. The error that results if the compressibility correction is not applied is shown to be +11 m.p.h. for a 400-m.p.h. airplane at 25,000 ft. altitude. The method here presented for applying the compressibility correction is less cumbersome than other suggested methods and has the additional advantage of retaining the use of the customary air-speed indicator calibration chart. Finally, the possible effect of compressibility on the position error of a pitot-static head installation is briefly analyzed and discussed, and the difficulties encountered in determining true atmospheric pressure and temperature in high-speed flight are mentioned.

INTRODUCTION

PERHAPS THE TITLE of this paper should more properly be "A Simple Method of Using the Complete Impact Pressure Equation in the Determination of True Air Speed" rather than its present title, for, actually, the procedure suggested in the following discussion is simply the correct application of a well-known and well-established law. The word correction arises from the fact that an approximating assumption has been in general use for so long a time that the error involved has been generally overlooked. Two assumptions are frequently made in dealing with air-stream velocities and impact pressures. One of these assumptions is that the impact pressure of the air upon coming to rest is proportional to the square of the velocity multiplied by the air density, and the second is that for a constant value of the impact pressure the product of the square of the velocity times the air density is always constant and independent of the separate values of pressure and temperature. It will be shown in the following discussion that the first of the above assumptions is not involved in the conventional method of determining true air speed but that the error that has been generally overlooked arises from the second of these assumptions. In order to appreciate satisfactorily the situation it is desirable to review the complete impact pressure equation and to examine the conventional procedure for calibrating the air-speed system of an airplane.

Presented at the Radio and Instruments Session, Tenth Annual Meeting, I.Ae.S., New York, January 28, 1942.

* Assistant Head of Aerodynamics and Flight Test Section, Vought-Sikorsky Aircraft Division.

THE IMPACT PRESSURE EQUATION

The usual air-speed indicating system in present-day airplanes consists of a pitot-static head located in the air stream and generally on the forward part of the wing or fuselage, connected by two tubes to an air-speed indicating instrument in the pilot's cockpit. The cockpit instrument contains a sealed diaphragm, suitably connected to an indicator hand, and is operated by the pressure difference between the total, or stop, pressure of the air stream and the static pressure, these pressures being transmitted by the pitot-static head.

The difference between the total pressure and the static pressure will be called the impact pressure, and it becomes apparent that the air-speed instrument is nothing more than a differential pressure gauge designed to be operated by the impact (differential) pressure of the air stream. For an incompressible fluid the impact pressure is given by the expression

$$p_t - p = \rho V^2/2 = q \qquad (1)$$

where

p_t = total, or stop, pressure
p = static pressure
ρ = air mass density
V = velocity of air stream
q = usual symbol for $\rho V^2/2$

The differential pressure expressed by the above equation is usually defined as the "dynamic pressure," and it is to be noted that the dynamic pressure so defined is the impact pressure of a fluid stream predicated on the assumption that the fluid is incompressible. The air of the atmosphere is not incompressible, however, and therefore Eq. (1) must be modified. As shown by Zahm,[1] the total pressure exerted by a moving air stream at the stagnation point of a body immersed in the air stream is

$$p_t = p\left[1 + \frac{(k-1)\rho V^2}{2kp}\right]^{k/(k-1)} \quad (2)$$

where the new symbol, k, is the ratio of specific heat of air at constant pressure to its specific heat at constant volume. This equation is derived from Bernoulli's equation for compressible flow with adiabatic compression, and the validity of the formula has been demonstrated by numerous experiments. For more readily comparing this equation with Eq. (1) it may be put in the following form, giving an expression for the impact pressure:

$$p_t - p = p\left\{\left[1 + \frac{(k-1)\rho V^2}{2kp}\right]^{k/(k-1)} - 1\right\} \quad (2a)$$

In order to show further the significance of this expression the term on the right may be expanded by the binomial theorem, at the same time substituting for $(kp/\rho)^{1/2}$ the symbol V_c, yielding the following:

$$p_t - p = (\rho V^2/2)\left[1 + \frac{1}{4}\left(\frac{V}{V_c}\right)^2 + \frac{(2-k)}{24}\left(\frac{V}{V_c}\right)^4 + \ldots\right] \quad (2b)$$

In Eq. (2b) the symbol V_c represents the velocity of sound in air and is related to atmospheric conditions as follows:

$$V_c = (kp/\rho)^{1/2} = a\sqrt{T} = \text{velocity of sound}$$

where T = absolute temperature and a = constant. It will be noted that the velocity of sound in air varies only with the temperature and, if T is in degrees centigrade (and for $k = 1.400$), the value of the constant a is 44.85, giving the velocity of sound in miles per hour.

Eq. (2b) shows that for compressible fluids the actual impact pressure is always greater than the "dynamic pressure," and Eq. (2a) shows that the relationship between the impact pressure, which will be designated q_c, and the dynamic pressure, q, is uniquely determined by p, the static pressure. (The specific heat ratio, k, is assumed constant over the normal range of atmospheric temperatures.)

Air-Speed Instrument Calibrations

At this point it appears desirable to explain how the dial of an air-speed indicator instrument is designed or calibrated. It is to be made clear that this immediate discussion applies only to the instrument itself and not to the overall flight calibration of the air-speed system, which includes the pitot-static head. The conventional differential pressure type of air-speed instrument can be designed to indicate the true value of the air speed only under one set of atmospheric conditions as determined by temperature and pressure independently. The Air Services of the United States Army and Navy in 1925 adopted the adiabatic formula of Eq. (2a) for the calibration of air-speed indicators[2] and selected standard sea-level atmospheric conditions for the definition of the temperature and pressure to be used in the formula. Consequently, for the marking of the instrument dial, Eq. (2a), after the substitution of standard sea level density and pressure, may be used to calculate the differential pressure corresponding to any value of the air speed, V. The value of the constant, k, is taken as 1.40 for air. A table of these differential pressures associated with various values of V at sea level is given in Table IV of reference 2, and it is not necessary to reproduce this table here. It will be noted that the compressibility of the air *is* taken into account in the calibration of air-speed instruments; however, difficulties immediately arise in making the proper interpretation of an instrument reading when this reading is obtained under atmospheric conditions differing from the standard sea-level conditions for which the calibration is made. Of course, it is appreciated that the air-speed instrument may be considered merely as a pressure gauge, and for a known value of the impact (differential) pressure as indicated by the pointer hand, Eq. (2a) may be used to solve for the true speed under any conditions of pressure and temperature. However, this process is cumbersome and tedious and is to be avoided if possible. The method by which such calculations may be avoided will be shown later, but before continuing it is desired to define the term true instrument air speed. "True instrument air speed" will be defined simply as the reading of a perfect instrument in a perfect installation—that is, the reading of a correctly calibrated instrument when subjected to the true impact pressure of the air stream. This definition merely fixes the relationship between true instrument air speed and the impact pressure according to the standard formula Eq. (2a), which has previously been explained.

Overall Calibration of Air-Speed System

The overall calibration of the air-speed system of an airplane includes the functioning of both the pitot-static head installation and the cockpit instrument. A conventional air-speed indicating system, in general, never gives the correct value of the indicated air speed, so an overall calibration of the system is always necessary. It will be immediately necessary to define the term "indicated air speed." The usual and simple definition of indicated air speed, which will be used here, is that indicated air speed is the product of the true air speed and the square root of the relative density ratio—that is,

$$\text{indicated air speed} = V\sqrt{\rho/\rho_0} = V\sqrt{\sigma} \quad (4)$$

Rather than confuse the discussion with additional symbols, the symbol for indicated air speed will be its equivalent in symbol form—viz., $V\sqrt{\sigma}$. As a matter of interest, the author has been unable to find a formal definition of indicated air speed in N.A.C.A. literature. The definition used above, however, is the same as that

given in recent C.A.A. publications, and it appears desirable that this definition should be standardized by all agencies concerned. It will be brought out later, however, that even a perfect air-speed indicator instrument in a perfect installation will not indicate true indicated air speed except under the special condition of sea-level pressure.

If the above definition of indicated air speed is accepted, and the differences between instrument air speed and true indicated air speed are investigated, then the errors in a conventional installation may be classified as follows: (1) position error of the pitot-static head, (2) calibration error of the air-speed instrument, (3) compressibility error, and (4) lag and acceleration error. It is necessary to understand these usual errors in order to fully appreciate the possible effects of compressibility. Item (4), however, which involves changes in altitude and changes in speed, will not be considered here. The present discussion will be confined to level flight, steady state conditions.

(1) The position error, or installation error as it is sometimes called, is concerned with the pitot-static head and its location. The error arises from the fact that either the pitot tube may not be transmitting the true total pressure of the air stream or the static tube may not be transmitting the true static pressure of the air stream; or the error may be due to a combination of these conditions. A properly designed pitot-static head, when placed in a uniform air stream with the flow parallel to the axis of the tube, will normally transmit the total pressure and the static pressure of the air stream with satisfactory accuracy. And, furthermore, such a head is reasonably insensitive to small angles of pitch up to 8 or 10 deg. This is equivalent to saying that the constant of a well-designed head may be considered unity over a limited range of pitch angles. A pitot-static head mounted on an airplane, however, is of necessity so close to either the wing or fuselage or some other part of the airplane that it is definitely in a region of flow which is influenced by the adjacent part of the airplane. The local flow at the pitot-static head, in general, does not have either the same velocity or the same static pressure as the free air stream, and the flow is usually at some angle to the axis of the tube. The pitot orifice, however, transmits the total pressure of the air stream, which is the sum of the impact and the static pressures; since this sum is always constant in streamline flow—i.e., flow for which Bernoulli's equation is applicable—the pitot tube gives a correct indication of the total pressure regardless of the local value of the velocity and of the static pressure. The local static pressure that exists at, and is transmitted by, the static tube is, in general, not the true static pressure of the undisturbed air stream. Consequently, the differential pressure transmitted by the pitot-static head is usually not the true impact pressure of the free air stream. In the high-speed range of airplanes the local angle of attack is generally small and, if the tube is relatively insensitive to pitch angles, no appreciable error will result from this source. Therefore, it may be concluded that the primary source, and usually the only source, of the installation error is the incorrect static pressure that is transmitted by the static tube from the pitot-static head.

The above discussion must be considered to apply to the operation of the pitot-static head in its subcritical flow regime—that is, below the speed at which a compressibility shock wave is formed near the nose of the tube. Experiments on typical pitot-static tubes[3,4] show that the correct total pressure is transmitted by the pitot orifice up to the sonic velocity, but the pressure at the static orifices begins to depart appreciably from the correct static pressure at a Mach number in the range from 0.72 to 0.80. Reference 4 satisfactorily correlates this error in static pressure at high Mach numbers with the formation of a shock wave near the nose of the tube and forward of the static orifices. It is felt that this error should be classed as a change in the constant of the pitot-static head rather than as an installation error, and although it is definitely a compressibility phenomenon it should not be confused with the subcritical compressibility error, item (3), which will be explained later. At the present time the level flight, maximum speeds of airplanes are not high enough to exceed the critical speed of the pitot-static head; however, the maximum diving speeds of modern fighter and pursuit airplanes are now reaching a range where possible errors from this source must be given consideration. Since the discussion of this paper, as stated previously, is confined to level flight conditions, the constant of the pitot-static head will be taken as unity and no further reference will be made to errors arising from supercritical velocities.

(2) The calibration error of the air-speed instrument is simply the error that may exist between the specified position of the indicating hand (according to the calibration formula) and the actual position of the hand for a given differential pressure on the instrument. This may be due to small errors in marking the dial, or it may be due to faulty mechanical operation of the instrument mechanism. For the sake of completeness, temperature errors should also be mentioned here. Even though modern instruments are designed with temperature-compensating devices, there may be a small but appreciable change in calibration when the temperature of the instrument is varied over a wide range.

(3) The compressibility error is defined as the difference between the true instrument air speed and the indicated air speed, $V\sqrt{\sigma}$. Perhaps this difference should not be classed as an error at all, for it is evident that if the overall errors of an air-speed system had been defined as the difference between the instrument air speed—i.e., the observed reading of a given instrument—and the true instrument air speed this so-called compressibility error would not have appeared at all.

Nevertheless, since indicated air speed as herein defined is a simple quantity from which the true speed may be readily obtained (after the density ratio is known), the determination of this quantity will be considered the primary aim of this paper. Consequently, the remainder of this discussion will deal with the isolation of the compressibility error and a means of readily applying it in the determination of indicated air speed.

The Compressibility Error

Indicated air speed is a direct function of $\rho V^2/2$ or q, since

$$V\sqrt{\sigma} = V\sqrt{\rho/\rho_0} = \sqrt{2q/\rho_0} \tag{5}$$

where ρ_0 = standard sea-level density = constant. Now, referring to Eq. (2a), it will be recalled that when standard sea-level values of pressure and density are substituted in this equation it becomes the formula for the design calibration of air-speed instruments. Consequently, under sea-level conditions of pressure and temperature it is apparent that true air speed and true instrument air speed will be identical. Also, since at sea level σ is equal to unity, it is evident that indicated air speed will have the same value as true air speed. Therefore, it develops that under standard sea-level conditions true air speed, true instrument air speed and indicated air speed are all the same. Now, let sea-level pressure be retained and investigate what changes take place when the atmospheric temperature is varied. The investigation will be made *at a constant value of the impact pressure;* therefore, since the true instrument reading is a function only of impact pressure, the true instrument air speed will remain constant. It is obvious that if the temperature is varied and the pressure held constant the density, ρ, must vary. Eq. (2a) shows, however, that if p and the impact pressure are to remain constant the product ρV^2 must remain constant. And since indicated air speed is a direct function of ρV^2, then the indicated speed will remain constant also. It will be seen that the true speed as well as the density ratio must vary, however. This situation may be explained in a different way by the use of Eq. (2b). If the impact pressure—that is, $p_t - p$— and the quantity ρV^2 both remain constant, then it is apparent that the term in the brackets on the right must also remain constant and that the ratio of V/V_c must remain unchanged. If ρV^2 remains constant with varying temperature, then V^2 must vary as T, the absolute temperature, since ρ is proportional to p/T. This variation, however, is exactly the variation shown for V_c by Eq. (3). Consequently, the ratio of V/V_c in the bracket of Eq. (2b) is unchanged, which is in accord with the indications from Eq. (2a). The main point to be noted here is that at a constant value of the impact pressure, the Mach number, i.e., the ratio V/V_c, is independent of temperature; consequently, if the Mach number changes at all it must vary with the pressure only. Before passing to the case of varying pressure, it will be observed that under the conditions of sea-level pressure the true instrument air speed and the indicated air speed are the same, regardless of the value of the temperature.

For the case of changing static pressure, p, which represents a variation of altitude, it is desirable to obtain some convenient relation between true instrument air speed and indicated air speed. This relation will be sought at a constant value of the impact pressure, and it is to be noted that if the impact pressure is constant the true instrument air speed will remain constant. Reference will again be made to Eq. (2a). It has been shown that indicated air speed is a simple function of ρV^2. Eq. (2a) may be rearranged for a solution of ρV^2, at the same time substituting for the impact pressure, $p_t - p$, its symbol, q_c, and the following is obtained:

$$\rho V^2/2 = \frac{kp}{k-1}\left[\left(\frac{q_c}{p}+1\right)^{(k-1)/k} - 1\right] \tag{2c}$$

and the indicated air speed is

$$V\sqrt{\sigma} = \left\{\frac{2kp}{(k-1)\rho_0}\left[\left(\frac{q_c}{p}+1\right)^{(k-1)/k} - 1\right]\right\}^{1/2} \tag{2d}$$

Let $V_1\sqrt{\sigma_1}$ represent the indicated air speed under sea-level conditions of pressure. Then

$$V_1\sqrt{\sigma_1} = \left\{\frac{2kp_0}{(k-1)\rho_0}\left[\left(\frac{q_c}{p_0}+1\right)^{(k-1)/k} - 1\right]\right\}^{1/2} \tag{2e}$$

and the ratio of indicated air speed at any pressure, p, to the indicated air speed at sea level pressure, p_0, is

$$\frac{V\sqrt{\sigma}}{V_1\sqrt{\sigma_1}} = \left\{\frac{p\left[\left(\frac{q_c}{p}+1\right)^{0.2857} - 1\right]}{p_0\left[\left(\frac{q_c}{p_0}+1\right)^{0.2857} - 1\right]}\right\}^{1/2} \tag{6}$$

where the exponent 0.2857 is the value of $(k-1)/k$ when k is equal to 1.40. The values of this equation have been computed for various values of q_c and p, covering a range of q_c represented by true instrument air speeds from 200 to 600 m.p.h. and a range of p represented by pressure altitudes from sea level to 40,000 ft. The calculated values are presented in Table 1 to four significant figures, which permits the calculation of the indicated air speeds at altitude to $^1/_{10}$ m.p.h. when so desired. Table 2 is an extension of the data of Table 1, showing values of indicated air speed at altitude for constant values of the impact pressure, as represented by various indicated air speeds at sea level. It will be noted that blank spaces are left in both tables in the lower right-hand corner in the high-speed, high-altitude region. This is done because the true air speeds represented by these spaces are above the speed of sound, in which region the applicability of the basic

TABLE 1

RATIO OF INDICATED AIR SPEED AT ALTITUDE TO INDICATED AIR SPEED AT SEA LEVEL, AT CONSTANT VALUES OF THE IMPACT PRESSURE. INDICATED AIR SPEED = $V\sqrt{\sigma}$

Standard Pressure Altitude (Ft.)	Values of Indicated Air Speed at Sea Level. $V_1\sqrt{\sigma_1}$, M.P.H.								
	200	250	300	350	400	450	500	550	600
Sea level	1.0000	1.0000	1.0000	1.0000	1.0000	1.0000	1.0000	1.0000	1.0000
5,000	0.9982	0.9975	0.9963	0.9953	0.9938	0.9923	0.9907	0.9890	0.9873
10,000	0.9960	0.9939	0.9916	0.9889	0.9859	0.9827	0.9793	0.9758	0.9723
15,000	0.9935	0.9902	0.9862	0.9817	0.9769	0.9717	0.9664	0.9608	0.9552
20,000	0.9901	0.9851	0.9791	0.9727	0.9666	0.9583	0.9507	0.9430	
25,000	0.9860	0.9790	0.9708	0.9619	0.9524	0.9426	0.9326		
30,000	0.9809	0.9713	0.9606	0.9492	0.9365	0.9240			
35,000	0.9743	0.9617	0.9478	0.9329	0.9176				
40,000	0.9660	0.9499	0.9323	0.9140					

TABLE 2

VALUES OF INDICATED AIR SPEED AT ALTITUDE, AT CONSTANT VALUES OF THE IMPACT PRESSURE

Standard Pressure Altitude (Ft.)	Indicated Air Speed at Sea Level. $V_1\sqrt{\sigma_1}$ = M.P.H.								
	200	250	300	350	400	450	500	550	600
Sea level	200	250	300	350	400	450	500	550	600
5,000	199.6	249.4	298.9	348.3	397.5	446.5	495.4	544.0	592.4
10,000	199.2	248.5	297.5	346.1	394.3	442.2	489.7	536.7	583.4
15,000	198.7	247.5	295.9	343.6	390.7	437.3	483.2	528.4	573.1
20,000	198.0	246.3	293.7	340.4	386.7	431.2	475.4	518.6	
25,000	197.2	244.7	291.2	336.7	380.9	424.2	466.3		
30,000	196.3	242.8	288.2	332.2	374.6	415.8			
35,000	194.9	240.4	284.3	326.5	367.0				
40,000	193.2	237.5	279.7	319.9					

Eq. (2) is doubtful.[1,4] The data of Table 2 are plotted in Fig. 1 as indicated air speed versus true instrument air speed, the latter being identical to $V_1\sqrt{\sigma_1}$. It will be observed in Fig. 1 that true instrument air speed has a different calibration—in terms of indicated air speed—for each value of the pressure altitude, which represents a certain value of the static pressure, p. The magnitude of the effect of pressure altitude on indicated air speed, for a given value of instrument air speed, will be shown by an example. For the case of 400 m.p.h. true air speed at 25,000 ft. ($\sigma = 0.4480$) the indicated air speed is 268 m.p.h., and from Fig. 1 the true instrument air speed is 275 m.p.h. If, however, for an instrument air speed of 275 m.p.h. the indicated air speed were read from the sea-level curve, giving an indicated air speed also of 275 m.p.h., the true speed at 25,000 ft. would be computed at 411 m.p.h., resulting in an overestimation of the true speed by 11 m.p.h. This error, as indicated by the curves of Fig. 1, is less for lower altitudes and speeds but greater for higher altitudes and speeds.

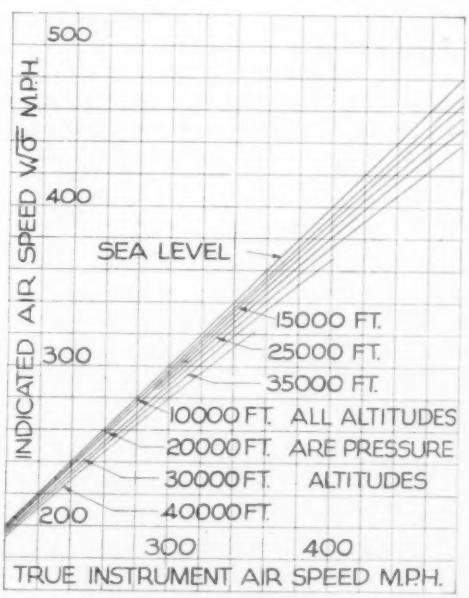

FIG. 1. Indicated air speed vs. true instrument air speed for various pressure altitudes.

It will be observed that the calculations of Tables 1 and 2 are based on a value of 1.40 for the specific heat ratio, k. The value of k, for dry air, found in various sources ranges from 1.40 to 1.41, and it appears that this ratio is actually a function of temperature, though the variation is extremely small (of the order of a few tenths of 1 per cent) over the range of temperatures encountered in the atmosphere. The value of 1.40 used here is consistent with that used in N.A.C.A.

publications. Check calculations for the case of 275 m.p.h. true instrument air speed show that a change in k from 1.40 to 1.41 results in an increase in indicated air speed of less than $^1/_{10}$ m.p.h. at 25,000 ft.

Flight Calibration of Air-Speed System

It has previously been shown that the several errors that may exist in an air-speed system make it necessary to obtain an overall calibration that will include the errors of the pitot-static head as well as the errors of the cockpit instrument. Such calibrations are generally made in flight, and the usual procedure is to fly the airplane over a speed course at various constant instrument air speeds and at the same time make observations, through facilities that are independent of the airplane's conventional air-speed system, from which the airplane's true air speed, as well as atmospheric pressure and temperature at the flight level, may be determined. From these data it is possible to compute true indicated air speed—that is, $V\sqrt{\sigma}$. If desired, the true impact pressure of the free air stream may also be calculated by means of Eq. (2a). The usual procedure, however, is to plot true indicated air speed against observed instrument air speed and obtain a curve that will give a relationship between these two speeds for any value of the instrument reading. A typical curve of this type for a monoplane on which the pitot-static head is mounted forward of the leading edge of the wing is shown in Fig. 2, labeled speed course calibration. The existence of an appreciable position error will be noted if it is assumed that the instrument error is small, as is usually the case. After such a curve of indicated air speed versus instrument air speed is obtained, it has been customary in the past to assume that this curve was applicable for flight at all altitudes and that for any condition of level flight the true air speed could be determined simply on the basis of the density ratio and the indicated air speed from this curve. As soon as it is appreciated, however, that the cockpit instrument is operated essentially on the basis of an impact (differential) pressure and that a constant value of the observed instrument air speed indicates a constant value of the impact pressure of the free air stream, it becomes apparent from the previous discussion of the relationship between instrument air speed and indicated air speed that the above assumption is in error. Although this error was negligible for slow-speed, low-altitude airplanes, it cannot be neglected in the accurate speed determination for high-speed airplanes operating at high altitudes.

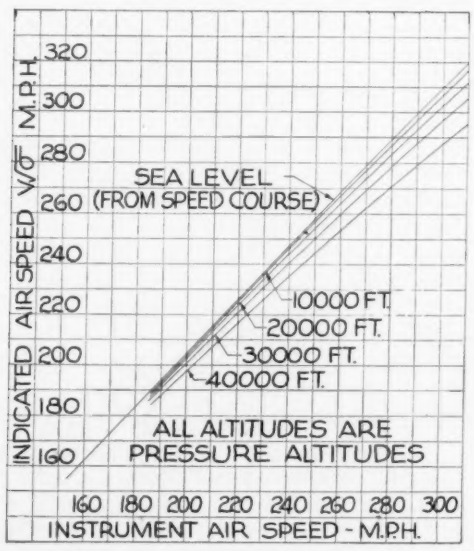

Fig. 2. Typical calibration chart for an air-speed system; indicated air speed vs. observed instrument air speed.

It remains now to show how the compressibility correction to indicated air speed which has previously been computed may be applied to the speed course calibration of the overall air-speed system. The correction is made at a constant value of the instrument air speed, since this implies that the free stream impact pressure is constant. In order to apply the relations that have previously been computed it is necessary to know either the true instrument air speed or its equal, $V_1\sqrt{\sigma_1}$, since either of these quantities fixes the value of the impact pressure. If the speed course calibration is obtained under conditions of sea-level pressure, then $V_1\sqrt{\sigma_1}$ is immediately known, since the indicated air speed computed in the usual manner is identical to $V_1\sqrt{\sigma_1}$ in this case. Therefore, the data of Table 2 may be used directly, and curves of indicated air speed at other pressure altitudes may be constructed on the usual calibration graph by plotting the points from Table 2 at the values of the abscissa (instrument air speed) which correspond to the tabular values of $V_1\sqrt{\sigma_1}$ as indicated by the speed course calibration curve. Such a process has been carried out in Fig. 2 on the basis of the speed course calibration there shown, and calibration curves have been obtained for pressure altitudes up to 40,000 ft. in 10,000-ft. increments. These additional altitude curves of indicated air speed versus observed instrument air speed represent calibration curves that would have been obtained if a speed course calibration could have been made at each of these pressure altitudes and are to be used as such. Therefore, the procedure for determining the true air speed at any altitude for a given value of the observed instrument air speed is similar to that used in the past except that care must be taken to interpolate for the indicated air speed at the proper pressure altitude—that is, at the pressure altitude at which the instrument air speed was observed. The true air speed is then readily computed after the density ratio is determined from observations of atmospheric temperature and pressure.

In cases where the speed course calibration is obtained under atmospheric pressure conditions that vary appreciably from standard sea level, a correction may be necessary for the difference between the speed course

value of $V\sqrt{\sigma}$ and the corresponding values of $V_1\sqrt{\sigma_1}$. This probably may be done most easily by cross-plotting the data of Table 1 to obtain the ratio of $V\sqrt{\sigma}$ to $V_1\sqrt{\sigma_1}$ at any altitude. The process to be followed is essentially the same as that followed in constructing altitude curves from one obtained at sea level. It will be noted from an inspection of Table 1, however, that a relatively large departure from sea-level pressure will be required before this correction becomes large enough to be necessary.

Overall calibrations of air-speed systems are sometimes made by other means than flying the airplane over a speed course. One of these methods uses a special pitot-static head that is suspended at the end of a long cable at a sufficient distance below and behind the airplane to be free from important interference effects. Since the primary cause of concern is usually only the static pressure, the suspended head may be only a static tube, in which case the total pressure is measured by a pitot tube directly attached to the airplane. In either instance it is presumed that the true impact pressure of the free air stream is correctly obtained. In this method of overall calibration, probably the simplest procedure is to determine true instrument air speed from the measured values of the impact pressure and to plot this speed against the observed reading of the normal cockpit instrument. Then, since true instrument air speed is identical to $V_1\sqrt{\sigma_1}$, the procedure for constructing curves of indicated air speed for various pressure altitudes becomes exactly the same as that described for the speed course calibration made at sea level.

The author is familiar with two other methods[5, 6] of handling the compressibility correction in determining true air speed; however, it is felt that the method here suggested is less cumbersome than other methods and has the additional advantage of retaining the customary air-speed calibration chart used in the past. Furthermore, the magnitude of the correction involved is always readily apparent and the required interpolation is a minimum.

Effect of Compressibility on Position Error

In the foregoing discussion it has been assumed that for a given cockpit instrument air speed the true impact pressure of the undisturbed air stream was always constant, regardless of the altitude. This statement, of course, is restricted to a given airplane at a constant gross weight and assumes no change in the calibration of the air-speed instrument itself. In the general case where a position error of the pitot-static head exists, this assumption implies that the position error is constant as long as the instrument air speed is constant. Stated another way, the implication is that even though the differential pressure transmitted by the pitot-static head is not the same as the true impact pressure of the free stream these two differential pressures always bear a fixed relation to each other. The position error, as previously explained, is generally due to the interference of the airplane wing or fuselage on the local static pressure at the openings of the static tube, and this interference is a function of the lift coefficient or angle of attack and may also be a function of Mach number. The usual assumption in the past has been that as long as the instrument air speed remained constant the angle of attack and the lift coefficient, as well as the flow pattern about the airplane, all remained unchanged. As a matter of interest, however, it can be shown that when the instrument air speed remains constant and the altitude is varied the lift coefficient, as well as the angle of attack, actually undergoes a slight change. This is due to the fact that the Mach number changes with altitude. Assuming for the present a constant value of the impact pressure and a change in standard altitude from sea level to 25,000 ft., an investigation reveals the following typical relations:

Standard Altitude	Sea Level	25,000 Ft.
True instrument air speed	275 m.p.h.	275 m.p.h.
Indicated air speed, $V\sqrt{\sigma}$	275 m.p.h.	268 m.p.h.
True air speed	275 m.p.h.	400 m.p.h.
Velocity of sound	761 m.p.h.	693 m.p.h.
Mach number, M	0.361	0.577
q_c/q	1.033	1.086
$1/\sqrt{1-M^2}$	1.072	1.226
Lift coefficient	0.1550	0.1635
Slope of lift curve, $dC_L/d\alpha$	0.0700	0.0800
Angle of attack, absolute	2.21 deg.	2.04 deg.

A wing loading of 30 lbs. per sq.ft. is assumed, and the lift curve slope of 0.0700 is arbitrarily chosen for the sea-level case and then increased in proportion to the respective values of $1/\sqrt{1-M^2}$. It will be observed that the lift coefficient has increased 5.5 per cent, while the angle of attack has been reduced by 7.7 per cent; furthermore, these changes are accompanied, or caused, by a change in the flow pattern about the airplane. These changes are obviously small in absolute magnitude; nevertheless, they do indicate that there may also be a change in local static pressure at the pitot-static tube relative to free stream static pressure. In order to form some idea of the magnitude of the possible change in local static pressure at the static tube openings, and the effect of this change on instrument and true air speed, it will be assumed that the static pressure error has been found at sea level to correspond to a $\Delta p/q$ of $+0.10$, which is not an abnormal error for a pitot-static tube mounted ahead of a monoplane wing. The pressure error is here given in terms of the usual pressure coefficient as a function of q; however, it is well known that pressure coefficients of this type are a function of Mach number. On the basis of the present limited knowledge regarding compressibilty effects, it is generally assumed that for an aerodynamic body at a constant attitude relative to an air stream the stagnation pressure coefficients vary with Mach number as q_c/q, while all other surface pressure coefficients vary approximately as $1/\sqrt{1-M^2}$, where M is Mach

number. The impact pressure acting on the open end of the pitot tube is a stagnation pressure and is identical with q_c. This point is the basis of all the previous discussion of the compressibility error and is satisfactorily proved by experiment. Therefore, it becomes evident that if the static pressure error varies in any other manner except directly with q_c the position error will change with altitude. Continuing the comparison between sea level and 25,000 ft., if the static pressure error is proportional to q_c, the error expressed as a pressure coefficient will become (1.086/1.033) (0.10) = 0.1051. In this case the position error remains constant. If, however, the pressure coefficient varies as the factor $1/\sqrt{1 - M^2}$, then the coefficient at 25,000 ft. becomes (1.226/1.072) (0.10) = 0.1144. The ratio of the coefficient in the latter case to that in the former is 0.1144/0.1051 = 1.09. This means that the error in static pressure at the openings of the static tube has increased by 9 per cent, while the impact pressure on the pitot tube remained constant, which reduces the differential pressure acting on the air-speed meter and consequently results in a reduction of instrument air speed. The reduction in differential pressure would amount to 1 per cent, corresponding to approximately $^1/_2$ per cent reduction in instrument air speed, and this change would take place, according to the conditions of the investigation, at a constant value of the true impact pressure of the free air stream. Consequently, the true air speed would be underestimated by approximately $^1/_2$ per cent, and, although this is a small percentage, it amounts to 2 m.p.h. true air speed in this selected case. If the assumed error in the static pressure at the static tube had been negative, then the true air speed would be overestimated by 2 m.p.h.

The above computations are obviously approximate and are intended only to point out the possibility of the small error that may be involved in the assumption that the true impact pressure is constant at all altitudes as long as the instrument air speed is constant, even though the pitot-static head has a position error. Under the circumstances, however, it appears that sufficient information to warrant any other assumption is not available. Obviously, the smaller the position error, the smaller will be the error resulting from changing altitude and, if there is no position error, the point of this discussion disappears entirely.

Determination of Density Ratio

Only brief mention has been made in this paper regarding the determination of the density ratio, σ, which is required in computing the true air speed after the indicated air speed is known. The determination of the density ratio requires a knowledge of the true atmospheric pressure and temperature at the flight altitude and, while this subject is not strictly within the scope of this paper, it is desired to point out that these two quantities are not easily obtainable with satisfactory accuracy in high-speed flight. It is customary to connect the altimeter to the static line from the pitot-static head, and when this is done it immediately becomes apparent that the pressure altitude that is indicated by the altimeter is subject to the same pressure error that is reflected as a position error of the pitot-static head. While the error in pressure altitude from this source is relatively unimportant with regard to determining the compressibility correction to indicated air speed, this error can be of definite significance in the determination of the true density ratio. Also, the usual thermometer that is carried on an airplane for measuring the free air temperature is always subject to a temperature rise due to compressibility effects. And this temperature rise is generally large at high velocities. Unless these two usual errors are properly appreciated and allowed for, they can readily result in errors in the true air speed of the same order of magnitude as those resulting from the neglect of the compressibility error.

References

[1] Zham, A. F., *Pressure of Air on Coming to Rest from Various Speeds*, N.A.C.A. T.R. No. 247, 1926.

[2] Beij, K. Hilding, *Aircraft Speed Instruments*, N.A.C.A. T.R. No. 420, 1932.

[3] Lock, C. N. H., and Hilton, W. F., *Calibration of Standard Pitot-Static Heads in the High-Speed Tunnel*, British Air Ministry R. & M. No. 1752, August, 1936.

[4] Walchner, O., *The Effect of Compressibility on the Pressure Reading of a Prandtl Pitot Tube at Subsonic Flow Velocity*, N.A.C.A. T.M. No. 917, November, 1939.

[5] Thompson, F. L., *The Measurement of Air Speed of Airplanes*, N.A.C.A. T.N. No. 616, October, 1937.

[6] Kotcher, Ezra, *The Compressibility Factor in Converting Indicated to True Air Speed*, U.S. Air Corps Technical Report No. 4515, February 29, 1940, unrestricted.

Propeller Forces Due to Yaw and Their Effect on Airplane Stability

L. B. RUMPH,* R. J. WHITE,† AND H. R. GRUMMANN‡

Curtiss-Wright Corporation

ABSTRACT

Forces produced by a propeller operating at an angle to the air-stream or being subjected to certain displacement velocities with respect to the air stream were calculated by Harris and Glauert in 1918. Recent tests on a propeller of modern plan form has shown that the theory of Harris and Glauert when used *without their empirical constant* predicted only half of the force in yaw as indicated by the tests. A new theory is presented here which has improved the agreement between the predicted and measured values of one of the force derivatives for the propeller tested and is believed to be more desirable for design calculations.

This method is based upon the same assumptions used by Harris and Glauert but includes the modified lift produced by an airfoil when operating in an oscillating air stream. The equations are in a different form than given by Harris and Glauert—they depend mainly upon the propeller blade form and clearly indicate that propellers having a wide root chord section will produce a greater side force due to yaw than would be realized with a propeller blade having a narrow root chord. This is an interesting conclusion, since a high-altitude pusher-type airplane that will probably require a propeller with a wide root chord will be favored from the stability point of view in comparison with a similar tractor-type airplane.

INTRODUCTION

THE EXISTENCE OF FORCES produced by a propeller when the thrust axis is at an angle with respect to the air stream or when it is being subjected to an angular velocity with respect to the air stream has been known for some time. The basic theory of this subject was developed by Harris[1] for the case of the propeller side force due to angle of yaw, and it was extended to include the effect of angular velocities by Glauert.[2] This work was done in 1917 and 1918 and until recently has not been extensively used, since the forces in question have generally been of secondary importance. Present designs require more engine power, necessitating more and larger propellers that may be disposed in new positions on the airplane. These tendencies make the problem of airplane stability more dependent upon certain forces produced by the propeller.

Recent wind-tunnel tests of a powered wind-tunnel model provided a means of measuring the side force and yawing moment produced by a propeller. A comparison of these measurements with the theory of Harris and Glauert showed that at some values of V/nD the test results were approximately twice those indicated by the theory. For this reason a new method of analysis has been used and new equations found for two of the more important force derivatives. The new method of analysis gives, for the side force due to yaw, better agreement with test results than the equation of Harris. As the new equations depend mainly on the propeller planform, they are believed more practical from the standpoint of design usage.

Presented at the Aerodynamics Session, Tenth Annual Meeting, I.Ae.S., New York, January 30, 1942.

* Chief Aerodynamicist.

† Aerodynamicist.

‡ Aerodynamicist.

EQUATIONS OF HARRIS AND GLAUERT

As the original works of Harris and Glauert are not readily available, the basic equations of reference 2 will be summarized and presented in a form that is believed to be more convenient for airplane stability calculations. Glauert shows that the following forces will be produced by a propeller undergoing a displacement or motion of the thrust axis: (a) side force (normal to thrust axis) due to angle of yaw, (b) pitching moment due to angle of yaw, (c) side force due to an angular velocity of pitch, (d) pitching moment due to an angular velocity of pitch, (e) force along the thrust axis due to a change in the velocity in the direction of the thrust axis, (f) torque produced by the propeller due to a change in the velocity in the direction of the thrust axis.

These have been rewritten and presented in Table 1. All of the force derivatives have been expressed in terms of airplane dimensions using N.A.C.A. nomenclature and are written for a right-hand propeller having

TABLE 1

Propeller Force Derivatives Based on Theory of Harris and Glauert for Constant Speed Right-Hand Propeller

	Aerodynamic Derivative	Equation	Value of R
(a)	$\frac{dC_Y}{d\psi}$	$= \frac{D^2}{S} R_1$	$\frac{f}{\pi}\left[\frac{C_P}{J} - \frac{1}{2}\left(\frac{dC_P}{dJ}\right)_\beta\right]$
(b)	$\frac{dC_m}{d\psi}$	$= \frac{D^3}{St} R_2$	$\frac{1}{\pi}\left[\frac{C_T}{J} - \frac{1}{2}\left(\frac{dC_T}{dJ}\right)_\beta\right]$
(c)	$\frac{dC_Y}{d(qb/2V)}$	$= \frac{D^3}{Sb} R_3$	$\frac{1}{\pi J}\left(\frac{dC_P}{dJ}\right)_\beta$
(d)	$\frac{dC_m}{d(qb/2V)}$	$= \frac{D^4}{Sbt} R_4$	$\frac{f_1}{2J}\left(\frac{dC_T}{dJ}\right)_\beta$
(e)	$\frac{dC_x}{d(u/V)}$	$= \frac{D^2}{S} R_5$	$\frac{-4}{J}\left[\frac{C_T}{J} - \frac{1}{2}\left(\frac{dC_T}{dJ}\right)_{C_P}\right]$
(f)	$\frac{dC_l}{d(u/V)}$	= zero	

the airplane axes coincident with the propeller hub in order to simplify Table 1. In applying these formulas it is a simple matter to include the moments produced by the forces when the airplane axes are referred to the airplane c.g. In the case of a left-hand propeller Eqs. (b) and (c) will change sign, hence must be considered zero for the case of a dual rotating propeller. The calculations and formulas of reference 2 were, of course, for a fixed-pitch propeller but, with two exceptions, are applicable to a constant-speed propeller. For constant-speed propellers Eq. (f) becomes zero and Eq. (e), as given in Table 1, has been recalculated. All other derivatives may be applied either to a fixed-pitch or constant-speed propeller. In the equations of Table 1 for R_1, R_2, etc., the subscript β or C_P on a derivative indicates the variable held constant during the differentiation.

By letting q_r and t_r represent a factor proportional to the torque and thrust per unit length along the propeller blade (Eqs. (13a) and (24a)) values of f and f_1 used in R_1 and R_4 are given by the integrals

$$f = (2/\pi)\int_0^1 q_r(R/r)^2 d(r/R)/\int_0^1 q_r d(r/R) \qquad (1)$$

$$f_1 = \int_0^1 t_r(r/R)^2 d(r/R)/\int_0^1 t_r d(r/R) \qquad (2)$$

The equations of Table 1, together with a propeller chart, will permit the numerical values of the propeller force derivatives to be readily calculated by graphically measuring the necessary propeller coefficient derivatives. The formulas of this table may be used, of course, to calculate the force derivatives about other airplane axes by a proper interchange of the axes.

In this paper the force derivatives (a) and (d) will be discussed in detail and new values of R_1 and R_4 will be determined by a different method. In addition, experimental values of (a) will be compared with values computed by the Glauert formula of Table 1 and by the new formula.

Side Force Produced by a Propeller in Yaw

In this analysis it will be assumed that a right-hand propeller is being sideslipped to the right, giving rise to a negative angle of yaw of the thrust axis but having a positive sideslip velocity. The rear view of this propeller is shown in Fig. 1. The vector marked $-V\Psi$ indicates that the propeller hub is moving to the right normal to the airplane flight velocity at a side velocity $-V\Psi$ where Ψ is the angle of yaw measured in radians. It will be assumed that all radial velocity components at the propeller blade may be neglected, which has been the assumption of all previous analyses. Fig. 2 shows the velocity vectors acting on the blade element indicated in Fig. 1 for the propeller blade in positions A and B. For the blade in position A no effect of the side velocity is experienced; therefore, the force coefficients will be denoted by the subscript $_0$ and will correspond to those for zero yaw.

During the motion from A toward B it will be assumed that the lift coefficient changes in magnitude and direction but that the drag coefficient changes only in its direction. This implies that the profile drag for zero yaw condition is unchanged. Let ΔC_s and ΔC_z be the changes in the force coefficients of the blade element normal to the radius in the plane of the propeller and normal to the plane of the propeller, respectively. Then by taking $\Delta\alpha$ negative as shown in Fig. 2 and of a small magnitude, $\cos\Delta\alpha = 1$, $\sin\Delta\alpha = \Delta\alpha$, giving

$$\begin{aligned}\Delta C_s &= C_s - C_{s_0}\\ &= (C_{L_0} + m\Delta\alpha)\sin(\phi-\Delta\alpha) + C_{D_0}\cos(\phi-\Delta\alpha) - \\ &\qquad (C_{L_0}\sin\phi + C_{D_0}\cos\phi)\\ &= (-C_{z_0} + m\sin\phi)\Delta\alpha \qquad (3)\\ \Delta C_z &= C_z - C_{z_0}\\ &= (C_{L_0} + m\Delta\alpha)\cos(\phi - \Delta\alpha) - \\ &\qquad C_{D_0}\sin(\phi - \Delta\alpha) - (C_{L_0}\cos\phi - C_{D_0}\sin\phi)\\ &= (C_{s_0} + m\cos\phi)\Delta\alpha \qquad (4)\end{aligned}$$

where

$$m = dC_L/d\alpha$$

Before proceeding with the integration of these force coefficients over the blade, the value of m will be established based upon Theodorsen's Eq. (18) of reference 3.

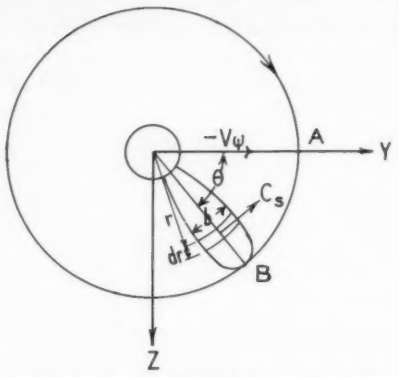

LOOKING FORWARD ALONG THRUST AXIS

Fig. 1.

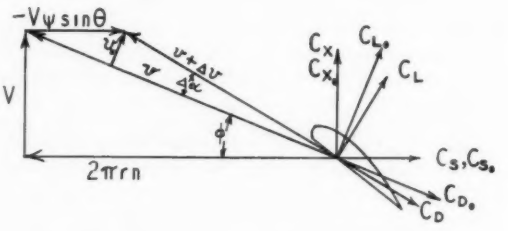

SECTION LOOKING FROM HUB TOWARD TIP FOR BLADE AT θ = 90°

Fig. 2.

A particular blade element in moving from A to B may be considered as an airfoil describing an oscillation normal and parallel to the direction of the undisturbed air velocity. Considering the oscillation normal to v, the vertical displacement velocity v_v of Fig. 2 may be written as

$$v_v = v\Psi \sin^2 \phi \sin \theta$$

Reversing the sign of Eq. (18) of reference 3 in accordance with the present notation and neglecting all terms not involving h or its derivatives, the lift coefficient ΔC_L becomes:

$$\Delta C_L = -P/(\rho/2)b'v^2 = [2\pi F \sin \theta + (\pi k + 2\pi G) \cos \theta]\Psi \sin^2 \phi \quad (5)$$

where

P = lift forces given by Eq. (18) of reference 3
b' = chord of blade element
k = $pb'/2v$
F, G = circulation functions of $1/k$ (see references 3 and 4)

In developing Eq. (5) the circular frequency is $p = 2\pi n$ where n = propeller speed (r.p.s.), and $pt = \theta$, making the amplitude of the relative displacement

$$h_0 = (b'/2k)\Psi \sin^2 \phi$$

It will be shown below that Eq. (5) must be multiplied by $\sin \theta$, and all terms having the product $\sin \theta \cos \theta$ will be zero when the average side force during one revolution is calculated; hence, at this point the $\cos \theta$ term will be dropped. From Fig. 2

$$\Delta\alpha = \Psi \sin^2 \phi \sin \theta \quad (6)$$

$$v = V/\sin \phi \quad (7)$$

But $m\Delta\alpha$ of Eqs. (3) and (4) is the lift coefficient ΔC_L of Eq. (5); hence

$$m = 2\pi F \quad (8)$$

The value of F is a function of the wing aspect ratio and of $1/k = J/\pi(b'/D) \sin \phi$, where (b'/D) is the ratio of the propeller total blade element width b' to propeller diameter D. In Fig. 3, curves of F are plotted for wing aspect ratios of ∞, 6, and 3, as taken from reference 4, and it is seen that for small values of $1/k$ the aspect ratio has little influence on F. In the present analysis the effect of aspect ratio will be neglected, all calculations being based upon the curve for aspect ratio of infinity.

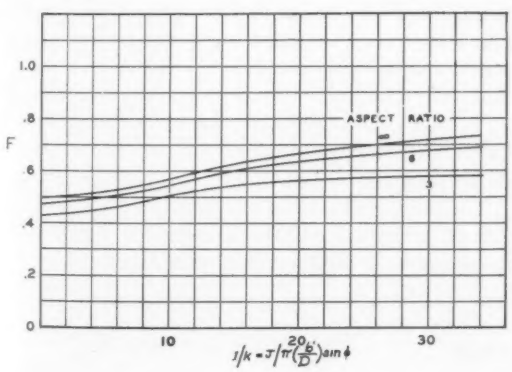

FIG. 3.

The value of m given by Eq. (5) is that experienced by an airfoil describing an oscillation normal to v, but the blade element is also moving fore and aft, giving rise to a change in the magnitude of v of the amount

$$\Delta v = v\Psi \sin \theta \sin \phi \cos \phi$$

or, combining with Eq. (6),

$$\Delta v/v = \Delta\alpha/\tan \phi$$

As this motion is in phase with the vertical oscillation, the value of m will be increased to include the effects of the change in the velocity v, which accompanies all changes in α. The value of m, however, will be referred to values of C_L based upon v. If C_{L_v} is the lift coefficient including the effects of the velocity $v + \Delta v$ but based upon v, then, as C_L is proportional to v^2 and α, the following differential expression may be written

$$\Delta C_{L_v}/C_{L_0} = (2\Delta v/v) + (\Delta\alpha/\alpha) = \Delta\alpha[(1/\alpha) + (2/\tan \phi)] \quad (9)$$

However, $C_{L_0} = m\alpha$; hence, the modified slope of the life curve m_v becomes

$$m_v = \Delta C_{L_v}/\Delta\alpha = m(1 + 2\alpha/\tan \phi) \quad (10)$$

For the purpose of this correction it is reasonable to assume that

$$C_{x_0} = C_{L_0} \cos \phi$$

which permits α to be written in terms of C_{x_0} giving

$$m_v = 2\pi F(1 + 2C_{x_0}/2\pi F \sin \phi)$$

Substituting m_v for m in Eq. (1)

$$\Delta C_s = (C_{x_0} \sin^2 \phi + 2\pi F \sin^3 \phi)\Psi \sin \theta$$

Referring to Fig. 1, the side force acting in the direction of the Y axis for the blade in position θ is

$$Y = \int_0^R (b'/D)D\,\Delta C_s(\rho/2)v^2 \sin \theta\, dr = (\rho/2)V^2(D^2/2)\Psi \sin 2\theta \int_0^1 (b'/D) \times (C_{x_0} + 2\pi F \sin \phi)\, d(r/R) \quad (11)$$

The above side force is periodic for a single blade, but, as the average side force is of interest here, the $\sin^2 \theta$ term may be replaced by its average value of one-half as

$$(1/2\pi)\int_0^{2\pi} \sin^2 \theta d\theta = 1/2$$

When this is done the average side force coefficient C_Y, based for convenience on the airplane wing area S, may be written for a propeller having B blades, as

$$C_Y = (BY)/(\rho/2)V^2S = R_1(D^2/S)\Psi \quad (12)$$

where

$$R_1 = (B/4)\int_0^1 (b'/D)C_{x_0}d(r/R) + (\pi/2)B\int_0^1 (b'/D) \times F \sin \phi d(r/R) \quad (13)$$

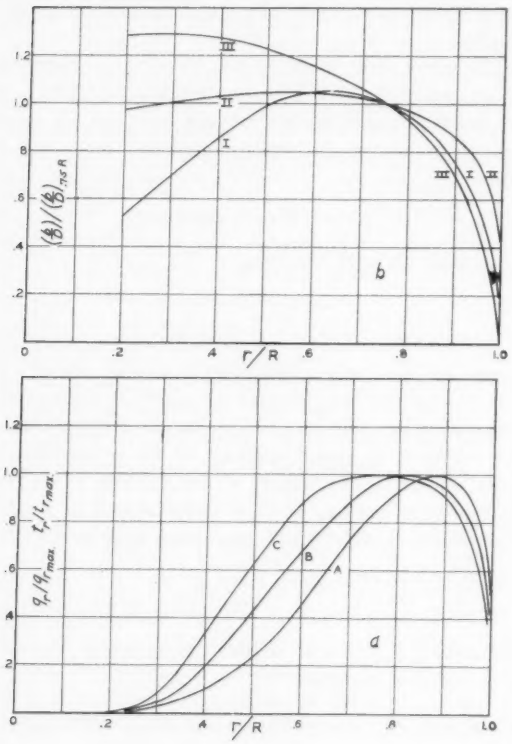

FIG. 4.

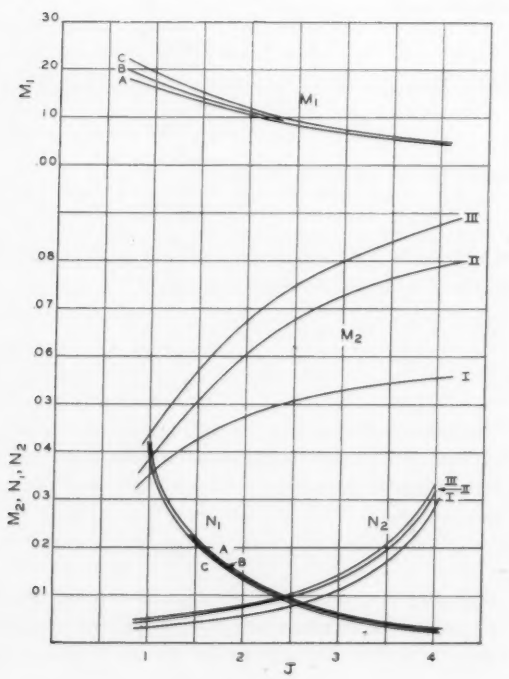

FIG. 5.

In order to get the first integral of R_1 in terms of the propeller thrust coefficient as measured for zero yaw, the thrust loading along the blade must be known if

$$t_r = (b'/D)C_{x_0}/\sin^2 \phi = \text{factor proportional to the thrust loading} \quad (13a)$$

then the propeller thrust T is

$$T = (\rho/2)V^2(D^2/2)B\int_0^1 t_r d(r/R) = \rho n^2 D^4 C_T \quad (14)$$

giving

$$(B/4)\int_0^1 t_r d(r/R) = C_T/J$$

The first integral of R_1 may now be written as

$$(B/4)\int_0^1 (b'/D)C_{x_0}d(r/R) = (B/4)\int_0^1 t_r \sin^2 \phi d(r/R) = M_1 C_P$$

where

$$M_1 = (1/J^2)\int_0^1 (t_r/t_{r_m}) \sin^2 \phi d(r/R) / \int_0^1 (t_r/t_{r_m})d(r/R) \quad (15)$$

The second integral of R_2 may be written as

$$(\pi/2)B\int_0^1 (b'/D)F \sin \phi d(r/R) = M_2 B$$

where

$$M_2 = (b'/D)_{0.75R}(\pi/2)\int_0^1 [(b'/D)/(b'/D)_{0.75R}] \times F \sin \phi d(r/R) \quad (16)$$

In order to determine M_1 and M_2, the thrust distribution and blade plan form for the propeller in question must be known. For values of J in the flight range the term M_1C_T is generally small in comparison to M_2B. This is fortunate since it enables an approximate thrust distribution to be used in determining M_1 and then M_2 may easily be calculated from the blade plan form.

In order to present values of M_1, three thrust distribution curves (later also to be used as torque distribution curves) have been arbitrarily selected and denoted by A, B, and C in Fig. 4a. These curves are not associated with any particular propellers, with the exception that curve A represents approximately the thrust distribution for the propeller used in the model tests. Values of M_1 for the thrust distributions A, B, and C are shown in Fig. 5. Likewise, M_2 as plotted in Fig. 5 has been calculated for three arbitrary propeller plan form distributions denoted by I, II, and III of Fig. 4b. These curves are not related to the curves A, B, and C and are based upon $(b/D)_{0.75R} = 0.0817$. Curve I represents an approximation to the plan form of the propeller tested.

The final equation for the side force coefficient, considered acting normal to the propeller thrust axis and based upon the airplane wing area, is

$$C_Y = R_1(D^2/S)\Psi \quad (17)$$

where

$$R_1 = M_1 C_T + M_2 B \quad (18)$$

Pitching Moment Due to an Angular Velocity of Pitch

This aerodynamic derivative is calculated because it is useful for longitudinal stability calculations. It is obtained in a manner similar to the previous derivation, except that an axial change of velocity is analyzed instead of a transverse one. When the propeller blade element is above the transverse Y axis located in the plane of the propeller at the propeller hub, a positive angular-pitch velocity q (rad. per sec.) will cause the forward velocity V at the blade element to be reduced; for the blade positions below the Y axis an increase in V will be realized. Combining velocity vectors similar to those shown in Fig. 2, a blade element will experience the following changes:

$$\begin{aligned} \Delta\alpha &= (-q_r/V)\sin\theta\sin\phi\cos\phi \\ \Delta v &= q_r\sin\theta\sin\phi \\ \Delta v/v &= -\Delta\alpha\tan\phi \end{aligned} \tag{19}$$

In this case, when the blade element encounters a positive change in $\Delta\alpha$, the value of Δv is decreased; hence, the value of m must be reduced in order to account for this variation in velocity. As an approximation let

$$\begin{aligned} C_{z_0} &= C_{s_0}/\tan\phi = C_{L_0}\cos\phi \\ C_L &= m\alpha \end{aligned}$$

then by using the first expression of Eq. (9)

$$\begin{aligned} n_v &= n[1 + 2(\Delta v/v)(\alpha/\Delta\alpha)] \\ &= 2\pi F[1 - 2C_{s_0}/2\pi F\cos\phi] \end{aligned}$$

Replacing this m_v for m in Eq. (4) in order to account for the effect of the change in v, the force coefficient of the blade element force parallel to the thrust axis now becomes

$$\Delta C_x = (C_{s_0} - 2\pi F\cos\phi)(qr/V)\sin\phi\cos\phi\sin\theta \tag{21}$$

The pitching moment for a propeller having B blades then becomes

$$M = (\rho/2)(D^3B/4)\int_0^1 v^2(b'/D)\,\Delta C_x(r/R)\sin\theta d(r/R)$$

Substituting Eq. (21) in Eq. (22) and replacing $\sin^2\theta$ by its average value of $^1/_2$, the pitching moment coefficient based upon the airplane wing area S and mean aerodynamic chord t is

$$\begin{aligned} C_m &= M/(\rho/2)V^2St \\ &= (D^4/Sbt)(qb/2V)\int_0^1(b'/D)(r/R)^2\times \\ &\qquad (C_{s_0} - 2\pi F\cos\phi)(1/\tan\phi)d(r/R) \end{aligned} \tag{23}$$

where b is the airplane wing span. However, $\tan\phi$ may be expressed as

$$\tan\phi = J/\pi(r/R)$$

giving

$$C_m = R_4(D^4/Sbt)(qb/2V)$$

where

$$\begin{aligned} R_4 = {} & (\pi b/8J)\int_0^1(b'/D)(r/R)^2C_{s_0}d(r/R) - \\ & \pi^2B/4J\int_0^1(b'/D)(r/R)^3F\cos\phi d(r/R) \end{aligned} \tag{24}$$

The first integral of R_4 will depend upon the torque distribution along the propeller blade.

Let

$$q_r = (b'/D)(r/R)(C_{s_0}/\sin^2\phi) = \text{factor proportional to the torque distribution} \tag{24a}$$

then the torque Q on the propeller at zero yaw may be written as

$$Q = (\rho/2)(V^2D^3B/4)\int_0^1 q_r d(r/R) = \rho n^2D^5(C_P/2\pi) \tag{25}$$

giving

$$\int_0^1 q_r d(r/R) = (4/\pi B)(C_P/J)$$

The first integral of R_4 then becomes

$$(\pi B/8J)\int_0^1(r/R)^2q_r\sin^2\phi d(r/R) = N_1C_P$$

where

$$N_1 = (^1/_2J^3)\ \frac{\int_0^1(r/R)^2(q_r/q_{r_m})\sin^2\phi d(r/R)}{\int_0^1(q_r/q_{r_m})d(r/R)} \tag{26}$$

The second integral of R_4 is written as

$$-(\pi^2B/4J)\int_0^1(b'/D)(r/R)^3F\cos\phi d(r/R) = -N_2B$$

where

$$\begin{aligned} N_2 = {} & (\pi^2/4J)(b'/D)_{0.75}\int_0^1[(b'/D)/(b'/D)_{0.75}]\times \\ & (r/R)^3F\cos\phi d(r/R) \end{aligned} \tag{27}$$

The final equation for the pitching moment coefficient produced by a propeller due to an angular velocity q about the transverse Y axis through the propeller hub is

$$C_m = R_4(D^4/Stb)(qb/2V) \tag{28}$$

where

$$R_4 = N_1C_P - N_2B \tag{29}$$

This expression has a form similar to that for the side force due to yaw. Using curves A, B, and C of Fig. 4a to represent the torque distribution along the propeller blade, values of N_1 have been computed and are plotted in Fig. 5. Values of N_2 were likewise computed and plotted using the plan forms I, II, and III of Fig. 4b.

Test Results and Comparison with Theory

The side force produced by a six-blade counter-rotating propeller has been determined from wind-tunnel tests on a powered wind-tunnel model. The effect of the running propeller was obtained by testing the model with and without the propeller. The model tested was such that any interference produced by the wing or fuselage was small. The side force acting at right angles to the propeller thrust axis was calculated and plotted against the angle of yaw, from which the values of $dC_Y/d\Psi$ were obtained from measurements of

TABLE 2

$\beta°$	J	C_T	M_1 Type B Propeller	M_2 Type I Propeller	Values of R_1 Test	Values of R_1 Glauert theory	Values of R_1 Present theory	Ratios of R_1's Test/Theory Glauert theory	Ratios of R_1's Test/Theory Present theory
30	1.33	0.075	0.13	0.040	0.296	0.171	0.251	1.73	1.18
30	0.965	0.225	0.18	0.034	0.296	0.191	0.244	1.55	1.21
38	1.5	0.192	0.137	0.042	0.383	0.225	0.278	1.70	1.38
38	1.61	0.145	0.13	0.043	0.395	0.221	0.277	1.78	1.42
38	1.04	0.315	0.172	0.036	0.309	0.206	0.270	1.50	1.14
46	2.12	0.20	0.104	0.0475	0.383	0.268	0.306	1.43	1.25
38	1.94	−0.035	0.113	0.046	0.321	0.206	0.272	1.56	1.18
38	1.95	−0.035	0.113	0.046	0.309	0.206	0.272	1.50	1.14
46	2.66	−0.10	0.082	0.051	0.321	0.353	0.298	0.91	1.08
46	2.68	−0.10	0.082	0.051	0.358	0.353	0.298	1.01	1.20

the average slope of these curves between 0 and 10 deg. angle of yaw.

The propeller tested had a diameter of $D = 2.25$ ft. and a plan form similar to curve I of Fig. 4b with $(b/D)_{0.75R} = 0.0817$. These tests results are tabulated in Table 2 in terms of R_1 along with the corresponding theoretic values of R_1.

The theoretic value of R_1 based upon Glauert's equation (Eq. (a), Table 1), was obtained by using the propeller coefficients measured in the wind tunnel. A value of $f = 1.44$ was determined by using curve B of Fig. 4a to represent the torque distribution. Strip calculations have shown curve B to be a good representation of the torque distribution for this propeller.

Theoretic values of R_1 determined by the present theory are also given in Table 2. These values were obtained by using M_1 and M_2 from Fig. 5 along with the measured thrust coefficients.

A comparison of these results is shown in Fig. 6, which represents the ratios of the test values of R_1 to the values calculated by Glauert's formula and by the present theory.

It appears that an empirical correction factor of approximately 1.2 would bring the theoretic values into good agreement with the test values. Pending the accumulation of more test results, no final value of such an empirical factor can be recommended.

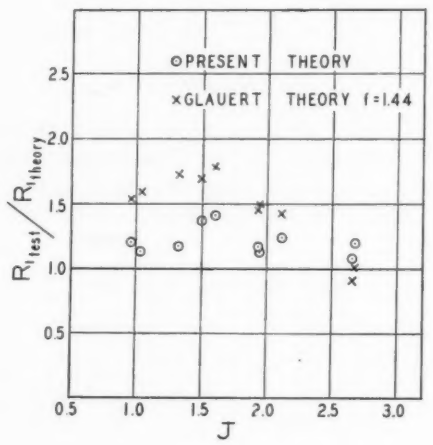

FIG. 6.

DISCUSSION

In this paper the theory of Glauert and Harris, which is based upon propeller coefficients, is compared with the present theory, which incorporates a correction to the blade element lift depending upon the theory of the oscillating airfoil. The present theory seems to be an improvement over that developed by Harris and Glauert and probably is a step toward obtaining a strictly rational formula. Before any conclusions on this point may be reached a further comparison with tests must be made.

The present theory has the advantage that it depends mainly on the propeller-blade plan form. As far as the side force due to yaw is concerned, it clearly indicates that propeller blades having large chords near the root will give the greatest side force due to yaw. The curves of Fig. 5 consist of values of M_1, M_2, N_1 and N_2 based upon three propeller-blade plan forms and thrust and torque distributions as shown in Fig. 4. The curves have been arbitrarily selected in order that, for any given propeller design, proper values of M_1, M_2, N_1 and N_2 may be estimated permitting the side force due to yaw and pitching moment due to pitch to be readily calculated.

REFERENCES

[1] Harris, R. G., *Forces on a Propeller Due to Sideslip*, R. & M. No. 427, February, 1918.

[2] Glauert, H., *Stability Derivatives of an Airscrew*, R. & M. No. 642, October, 1919.

[3] Theodorsen, T., *General Theory of Aerodynamic Instability and the Mechanism of Flutter*, N.A.C.A. T.R. No. 496, 1935.

[4] Jones, R. T., *The Unsteady Lift of a Wing of Finite Aspect Ratio*, N.A.C.A. T.R. No. 681, 1940.

A Practical Method of Allowance for Shear Lag*

JOHN DE S. COUTINHO†

Grumman Aircraft Engineering Corporation

SUMMARY

The calculation of stresses in a semimonocoque cantilever wing is discussed from an engineering-office point of view.

The influence of various factors on the stress distribution in thin-walled structures is considered, especially the effects of shear lag for which a simple empirical method of allowance is suggested. The use of the method is illustrated in the example of a box-beam wing, and the results of the calculations are checked by stress measurements on a full-size test specimen.

INTRODUCTION

IN PRACTICAL AIRCRAFT DESIGN the strength-weight ratio is a factor of primary importance. Efficient design requires a small but reliable margin of safety in all elements. Hence, a reasonably accurate knowledge of the stress distribution is essential.

In the commercial design of aircraft, however, the time element and the available mathematical skill often prohibit the preparation of intricate exact calculations. The value of a method that is to be of practical use will therefore depend greatly on its simplicity, flexibility, and the time and labor involved in obtaining reasonable answers.

This paper represents, therefore, an effort to contribute to the simple and practical empirical methods for the use of the skilled and experienced designer.

THE STRESS DISTRIBUTION IN A CANTILEVER BEAM

The design of a cantilever beam is based on the knowledge of the stress distribution in the various cross sections of the beam.

Consider the stress distribution in a cantilever prismatic beam of narrow rectangular cross section, Fig. 1. For $a \ll b$, the exact stress distribution is given as follows: normal stress, $\sigma = My/I$; shear stress, $\tau = PQ/bI$.

The normal stress distribution given in this expression is plane and represents the simplest bending stress distribution conceivable. The formulas are easily applicable, giving relatively simple calculations and quick results. The conception of planes before bending remaining planes after bending yields a descriptive mental picture that is easy to visualize and to work with.

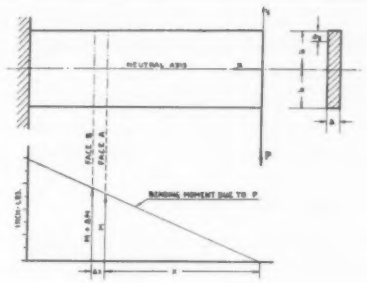

FIG. 1.

For even slight deviations from the narrow rectangular cross section, however, the formulas, in all cases for which an exact solution is known, become considerably more complicated, though the actual distribution may be similar. Since the possible gain in accuracy is out of proportion to the additional labor involved, the general practice is to assume plane stress distribution for all cases of bending. In the analysis of complex thin-walled structures this method may result in considerable error. The simple formulas are then applied to a modified and idealized substitute structure that is selected in such a manner as to give results that correspond with reasonable accuracy to the critical stresses in the actual structure.

The art consists in selecting the appropriate idealized substitute structure. Primary consideration should thereby be given to various factors listed in reference 1 as follows: (1) behavior of thin sheet in compression and as a shear web; (2) effects of shear lag; (3) effects of doors, windows, and similar cutouts.

1 The Behavior of Thin Sheet in Compression and as a Shear Web

The behavior of thin sheet in compression has been studied extensively elsewhere, and the problem is summarized in reference 1 as follows:

When a compressive load is applied to a stiffened panel in the direction of the stiffeners, the thin plate will be subjected to a stress of varying intensity. The intensity of this stress will tend to be a maximum at the stiffeners and a minimum midway between the stiffeners.

For convenience it is assumed that the thin sheet,

Received March 19, 1942.

* Based on a thesis submitted in partial fulfillment of the requirements for the degree of Master of Aeronautical Engineering, College of Engineering, New York University.

† Aeronautical Engineer.

which is under variable stress, can be replaced by effective widths of sheet w cooperating with each stiffener and subjected to the same stress as the stiffener, the rest of the sheet being considered ineffective—i.e., as carrying no load. The equation for computing the increments of effective width w can be expressed as follows:

$$w = Ct\sqrt{E/f_c}$$

where t is the thickness of the sheet and f_c is the stress in the stiffener. Values for the constant C for different types of sheet-stiffener combinations using aluminum alloys are given in reference 1.

The behavior of thin sheet acting as a shear web is discussed in references 2 and 3. Consideration of this effect is a refinement beyond the scope of this paper.

2 *Effects of Shear Lag*

In order to evaluate properly the effects of shear lag, it is necessary to have an understanding of the fundamentals of the phenomenon.

Consider the equilibrium of an element of a cantilever prismatic beam, as shown in Fig. 1, with a concentrated load P at the free end. The bending moment will be:

$$\text{Face A:}\quad Px = M$$
$$\text{Face B:}\quad P(x + \Delta x) = M + \Delta M$$

Element AB has been redrawn in Fig. 2 and divided into layers of infinitesimal thickness dy. The layers have been separated to show their reciprocal effects.

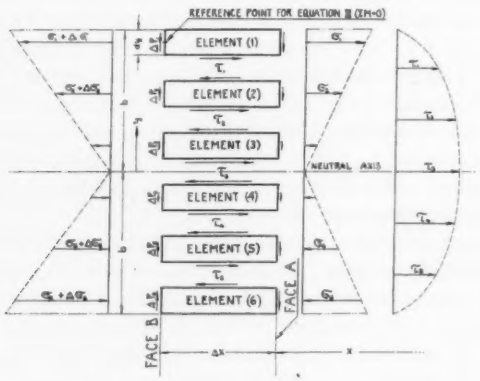

FIG. 2.

Normal stress distribution (plane):

$$\text{Face A:}\quad \sigma_A = My/I = \sigma$$
$$\text{Face B:}\quad \sigma_B = (M + \Delta M)y/I = \sigma + \Delta\sigma$$

Shear stress distribution (constant along x):

$$\tau = 0.5P(b^2 - y^2)/I$$

Equations of equilibrium for Element (1):

$$\Sigma X = -(\sigma_1 + \Delta\sigma_1)ady + \sigma_1 ady + \tau_1 a(\Delta x) = 0 \quad \text{(I)}$$
$$\Sigma Y = +\Delta P_1 - \Delta P_1 = 0 \qquad \text{(Note: } \Sigma\Delta P = P\text{)} \quad \text{(II)}$$
$$\Sigma M = \tau_1 a(\Delta x)dy/2 - \Delta P_1(\Delta x) = 0 \quad \text{(III)}$$

Eqs. (II) and (III) are of no further interest in the matter to be investigated.

In Eq. (I), the original component of the normal load $\sigma_1 ady$ is balanced between Face A and Face B longitudinally through Element (1) in pure tension.

The shear load $\tau_1 a(\Delta x)$ due to the change in normal load goes first into the neighboring Element (2), from there as a component of the shear load $\tau_2 a(\Delta x)$ into the next Element (3), and so on through the beam cross section, until it is finally balanced by the shear load $\tau_6 a(\Delta x)$ in Element (6). The shear load $\tau_2 a(\Delta x)$ goes through Elements (3) and (4) before it is finally balanced in Element (5).

In general the change in normal load in a given element is balanced by an equal change in normal load of opposite sign in an element of equal and opposite static moment about the neutral axis. Two such elements must therefore be connected in such a manner that an exchange of shear can take place.

In the narrow rectangular beam for which the normal stress distribution is plane, the shear load path between flanges is straight and sufficiently narrow to prevent a dissipation or redistribution of stresses over the constant width a. If, on the other hand, the flow of shear between flange elements is restricted and the internal distribution of longitudinal shear loads along the width a to the flange elements is disturbed, a deviation from the plane stress distribution is to be expected.

Consider, for example, the bending stresses in a channel as shown in Fig. 3. The shear load in Element (1) is ultimately balanced according to the conception advanced in the preceding paragraph by the shear load in Element (7). However, the shear load path between these two flange elements is not straight but leads around the corners through Elements (2), (3), (4), (5) and (6). Furthermore, all longitudinal shear loads between the flanges (i.e., between Elements (1), (2), (3) and Elements (5), (6), (7)) are balanced only through a thin web, represented by Element (4). This causes a concentration of shear loads in the thin web and constitutes a considerable restriction in the flow of shear as compared to the narrow rectangle. The normal stress distribution will therefore not be plane.

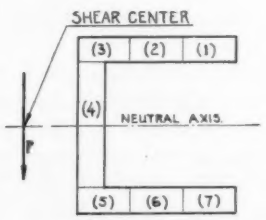

FIG. 3.

In the subsequent investigation of the stress distribution in a box-beam-type wing, the problem is reduced to the study of a channel, since by placing the open ends

of two channels together a symmetric box beam is formed.

Consider, therefore, the channel shown in Fig. 4 as the left half of a cantilever box beam. The applied load is assumed as acting at the shear center, causing pure bending. There will therefore, by definition of the shear center, be no rotational deflections of the beam, i.e., Element d will not deflect laterally and requires no support from the right half of the box beam, which is therefore justifiably cut away.

The channel is constructed of thin sheet and stiffened by the identical stiffeners a, b, c, d, which are equally spaced along the flanges.

Under the applied load shown in Fig. 4 the upper flange is in tension, which is applied to the flange by the web along stringer a. In Fig. 5 the longitudinal shear load applied by the web to the entire upper flange (ADEH) is designated by P_1.

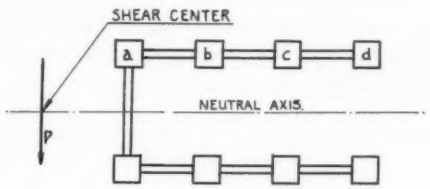

FIG. 4.

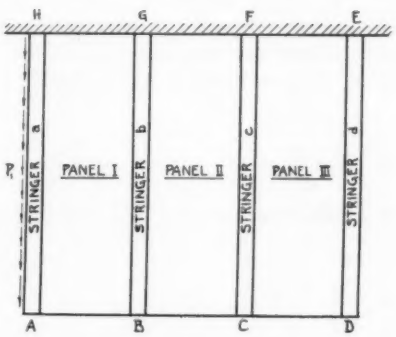

FIG. 5.

In Fig. 6 the flange ADEH is shown deflected under load, each element being isolated, with the vertical loads in equilibrium. Due to the continuous build-up of load along the fixed edge EFGH, stringer a shows the greatest deflection, stringers b, c and d being next in the order named. Hence, from Fig. 6:

$$AA' > BB' > CC' > DD'$$

Since by Hooke's Law the stress is proportional to the deflection, it follows that

$$\sigma_a > \sigma_b > \sigma_c > \sigma_d$$

where σ is the normal stress in the stringer designated by the subscript.

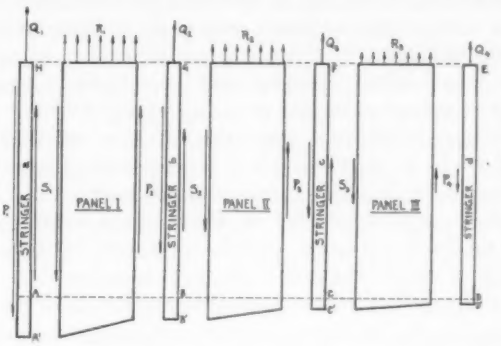

FIG. 6.

Since in Fig. 6

$$S_1 = S_2 + R_1 + Q_2$$

it follows that the load S_1 applied to Panel I is larger than the load S_2 applied to Panel II. The shear deflection of Panel I will therefore be greater than the shear deflection of Panel II, and the slope of A′B′ with respect to AB will be greater than the slope of B′C′ with respect to BC. Hence, the difference in deflection of stringers a and b will be greater than the difference in deflection of stringers b and c.

The same argument applies naturally to Panels II and III. Hence, in terms of linear deflections it follows that

$$(AA' - BB') > (BB' - CC') > (CC' - DD')$$

and, as above, in terms of stresses:

$$(\sigma_a - \sigma_b) > (\sigma_b - \sigma_c) > (\sigma_c - \sigma_d)$$

This equation for the character of the normal stress distribution in the flange is plotted in Fig. 7.

If area is added to the capstrip stringer a making this stringer relatively stiffer, its initial deflection AA′ will be smaller. Hence, the initial deflection of Panel I will also be smaller, as will that of Panel II and so on through the entire flange. Since all deflections are smaller, the stress in the entire flange will also be lower, as indicated in broken lines in Fig. 7. It should be noted, however, that notwithstanding the

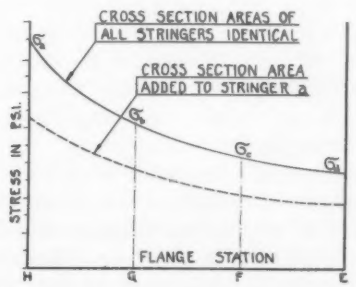

FIG. 7. Stress distribution in the flange.

lower stress in stringer a, the load Q_1 now carried by this stringer due to added area is larger than before, since the loads in all other stringers with unchanged areas are less, but the total load carried at each longitudinal station of the flange has not changed.

If area is added to any other stringer, the load Q taken out in that stringer is correspondingly greater and will cause a larger change in the angle of the deformed edge A′B′C′D′ at that stringer—the angle on the left being larger, and the one on the right being smaller, than in the case of identical stringers.

A change in stringer spacing will affect the stiffness of the panel—the closer the stringer spacing, the stiffer the panel and the smaller the drop in load carried by the neighboring stringer.

For the complete box beam, which, as stated above, is obtained by placing the open ends of two channels together, the normal stress distribution for bending about a horizontal and vertical axis will be as sketched in Fig. 8.

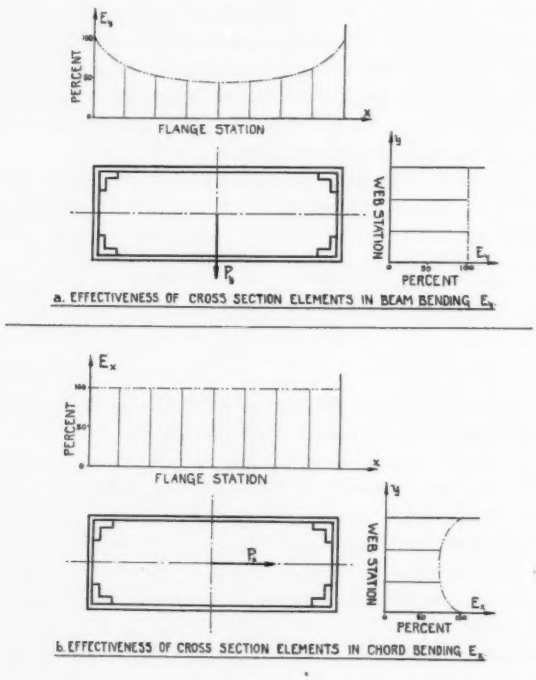
PERCENT
FLANGE STATION
WEB STATION
PERCENT
a. EFFECTIVENESS OF CROSS SECTION ELEMENTS IN BEAM BENDING
b. EFFECTIVENESS OF CROSS SECTION ELEMENTS IN CHORD BENDING

FIG. 8.

By calling the normal stress in the capstrips 100, the curves show the ratio of stress in any flange element relative to the capstrips and are therefore termed "efficiency curves." Numerical values taken from these curves are known as "efficiency factors."

In the analysis of a box-beam wing, such efficiency curves giving the character of the stress distribution can be sketched for various cross sections along the wing span. Spanwise plots of the efficiency factors along each stringer, which must be fair curves, will coordinate the various cross sections.

The efficiency factors E obtained from these curves are included in the standard bending stress computations as follows:

Moments of inertia:

$$I_x = \Sigma E_y A y^2$$
$$I_y = \Sigma E_x A x^2$$

Normal stresses:

$$\sigma_y = E_y M_x y / I_x$$
$$\sigma_x = E_x M_y x / I_y$$

3 *Effects of Doors, Windows, and Similar Cutouts*

By carrying the above reasoning a little further, efficiency curves may be drawn for sections through cutouts. The efficiency of discontinued stringers is naturally zero at the cut, while the efficiency of the stringers directly adjacent to a cutout will be considerably higher because of stress concentrations at the edges. The spanwise curves along the individual stringers must be faired carefully. However, the estimation of stress concentrations is beyond the scope of this paper.

The Stress Distribution in a Box Beam Wing as a Case Study

The application of efficiency factors is demonstrated for the case of the cantilever wing beam sketched in Fig. 9, which has a semispan of 21 ft. and a root chord of 6 ft. The wing consists of a center section and two outer panels. There are two engine nacelles in the center section. The material is Alcoa 24S-T throughout.

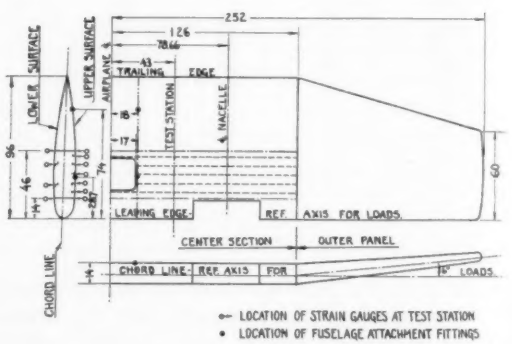

FIG. 9. Test specimen.

The center section is straight, of constant cross section (N.A.C.A. Airfoil 23015), having no taper, sweepback, or dihedral. The structure is semimonocoque, having two webs. The upper surface between the webs consists of two extruded plates with integral stiffeners. The plates are butt-jointed along the center of the box by a tee stringer.

The bending stresses in a critical loading condition are calculated for a representative cross section with

and without use of efficiency factors, and the computations are checked by actual stress measurements on a full-size test specimen.

Calculation of Stresses

Applied Loads

The applied loads on the wing at a station 43 in. outboard of the airplane centerline for a hydraulic test pressure of 700 lbs. per sq. in. are given in Fig. 10 in terms of the following components:

$$L = 8{,}944 \text{ lbs.}$$
$$D = -2{,}730 \text{ lbs.}$$
$$M_L = 1{,}926{,}600 \text{ in.lbs.}$$
$$M_D = -442{,}600 \text{ in.lbs.}$$

The pitching moment is not of interest and is neglected.

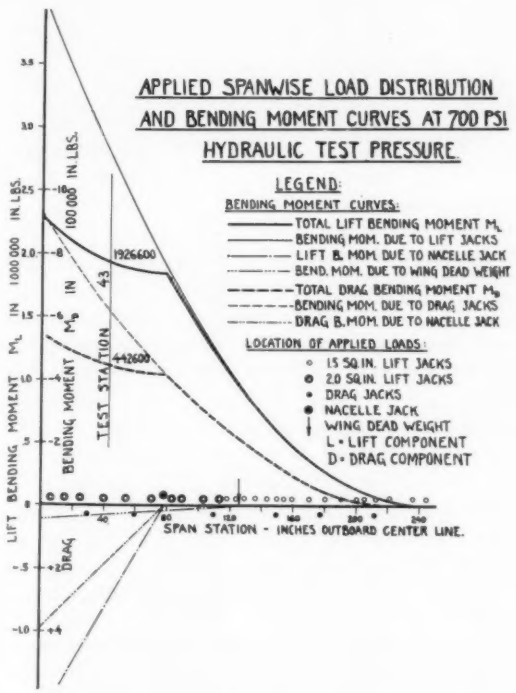
APPLIED SPANWISE LOAD DISTRIBUTION
AND BENDING MOMENT CURVES AT 700 PSI
HYDRAULIC TEST PRESSURE
LEGEND:
BENDING MOMENT CURVES:
TOTAL LIFT BENDING MOMENT M_L
BENDING MOM. DUE TO LIFT JACKS
LIFT B. MOM. DUE TO NACELLE JACK
BEND. MOM. DUE TO WING DEAD WEIGHT
TOTAL DRAG BENDING MOMENT M_D
BENDING MOM. DUE TO DRAG JACKS
DRAG B. MOM. DUE TO NACELLE JACK
LOCATION OF APPLIED LOADS:
15 SQ IN. LIFT JACKS
20 SQ IN. LIFT JACKS
DRAG JACKS
NACELLE JACK
WING DEAD WEIGHT
L = LIFT COMPONENT
D = DRAG COMPONENT
LIFT BENDING MOMENT M_L IN 1000 000 IN LBS.
100 000 IN LBS.
BENDING MOMENT M_D IN
1926600
442600
TEST STATION 43
DRAG
SPAN STATION - INCHES OUTBOARD CENTER LINE.

FIG. 10.

Selection of Critical Stresses

The closed type of box beam being studied here has a large included area, which is inherently rigid against torque; the torsional stresses are small and of no consequence.

The shear stresses must usually be carefully checked, but in small and medium-size airplanes the shear webs are inclined to be stronger than calculated by routine conservative engineering methods. Problems that may cause trouble here are likely to be limited to the design of efficient methods of connecting the shear webs to the flanges.

Since the beam-bending stress is an inverse function of the moment of inertia and the height of the wing beam is limited, bending strength is dependent on the amount of area in the flanges. Sufficient bending strength can be provided only at direct cost in weight. The chord bending will directly add to the beam-bending stress.

The bending stresses are therefore the primary design criterion and comprise the subject of the present limited investigation.

Estimation of Effective Areas

The trailing edge of the wing aft of the rear web is built of relatively thin sheet and will therefore carry negligible loads. The leading edge is extensively cut out so that major loads at station 43 cannot occur. All material forward of the front web and aft of the rear web will therefore be considered ineffective, and only the flange material between the two webs is assumed to carry load.

Because of its large thickness, the top cover is assumed to be totally effective in compression across its full width. The lower flange is assumed to be fully effective in tension across its full width.

The effective areas of the webs in compression are computed by the formula taken from reference 1 in heading No. *1*. The distribution of effective material is shown in Fig. 11.

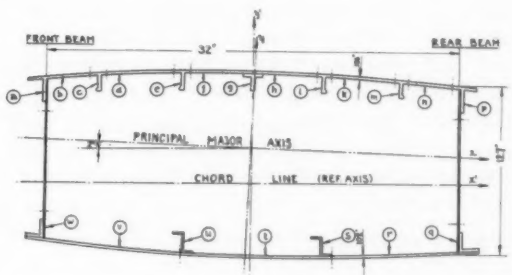

FIG. 11. Distribution of effective material in bending.

Estimation of the Effects of Shear Lag

Allowance for the effects of shear lag is made in the efficiency curves, Fig. 12. These curves were plotted after consideration of the arguments presented above, and they are claimed to be essentially correct in character. The choice of the numerical values is a matter of judgment and experience, such as the choice of the effective material.

Computation of Stresses

Normal bending stresses are computed from the values given in Tables 1 and 2 both by the standard method and by the suggested method allowing for the effects of shear lag. The results of the calculation are summarized in Table 3 and plotted in Fig. 13.

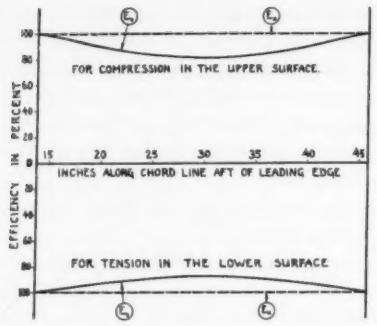
FOR COMPRESSION IN THE UPPER SURFACE
EFFICIENCY IN PERCENT
15 20 25 30 35 40 45
INCHES ALONG CHORD LINE AFT OF LEADING EDGE
FOR TENSION IN THE LOWER SURFACE

FIG. 12. Estimated efficiency curves for the effective cross section shown in Fig. 11.

TABLE 1

Geometric Values and Efficiency Factors

Element	Area A, Sq.In.	x', In.*	y', In.*	E_x, %	E_y, %
(a)	0.759	−16.0	7.2	100	100
(b)	0.490	−13.4	8.3	100	97
(c)	0.400	−11.4	7.95	100	93
(d)	0.780	− 8.4	8.6	100	88
(e)	0.400	− 5.4	8.15	100	84
(f)	0.760	− 2.4	8.6	100	82
(g)	0.234	0	8.0	100	81
(h)	0.760	2.4	8.5	100	82
(j)	0.400	5.4	7.8	100	84
(k)	0.780	8.4	8.16	100	88
(m)	0.400	11.4	7.43	100	93
(n)	0.490	13.4	7.76	100	97
(p)	0.655	15.95	6.70	100	100
(q)	0.474	16.1	−4.47	100	100
(r)	1.224	11.5	−5.5	100	94
(s)	0.152	5.4	−5.0	100	89
(t)	1.120	0	−5.7	100	86
(u)	0.152	− 5.4	−4.85	100	89
(v)	1.224	−11.5	−5.1	100	94
(w)	0.500	−16.05	−3.68	100	100
Total	12.154				

* x' and y' are measured from the reference axes, Fig. 11.

EXPERIMENTAL DETERMINATION OF STRESSES

Description of the Test Specimen

The actual bending stresses are determined on a full-size test model, consisting of a complete center section and a left outer panel. The right outer panel is replaced by a jury structure. The stresses are measured on the left side of the center section with Huggenberger Tensometers located on centerlines of the longitudinal members at and between the front and rear web cap-strips on both upper and lower surfaces (Fig. 9).

The model is supported by a jig at the wing-fuselage fittings.

Description of the Loading Equipment

The test loads are applied by hydraulic jacks. The applied jack-bending moments, Fig. 10, are corrected for the effects of wing dead weight.

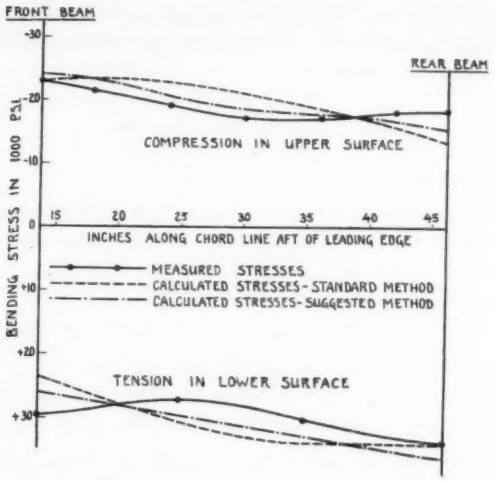
FRONT BEAM
REAR BEAM
COMPRESSION IN UPPER SURFACE
BENDING STRESS IN 1000 P.S.I.
15 20 25 30 35 40 45
INCHES ALONG CHORD LINE AFT OF LEADING EDGE
MEASURED STRESSES
CALCULATED STRESSES - STANDARD METHOD
CALCULATED STRESSES - SUGGESTED METHOD
TENSION IN LOWER SURFACE

FIG. 13. Stress distribution over the wing chord at 43 in-outboard from airplane centerline and at 700 lbs. per sq. in. hydraulic test pressure.

TABLE 2

Moments of Inertia and Applied Moment Vectors

Item		Standard Method	Suggested Method
Moments of inertia about	I_{x_1}	498.3	458.2
reference axes	I_{y_1}	1,368.4	1,368.4
Polar moment of inertia	$k = Ax_1y_1$*	−31.6	−31.4
Angle of principal axes	α†	−2° 4′	−1° 51′
Moments of inertia about	I_x	497.4	457.5
principal axes	I_y	1,368.3	1,370.9
Applied moment vectors about	M_L'	1,910,700	1,912,400
principal axes	M_D'	−511,300	−504,200

* Where $x_1 = x - (\Sigma Ax)/(\Sigma A)$ and $y_1 = y - (\Sigma Ay)/(\Sigma A)$.
† From $\tan 2\alpha = 2k/(I_{y_1} - I_{x_1})$.

TABLE 3

Calculated Stresses

Fiber	x, In.*	y, In.*	Normal Stress, Standard Method	Normal Stress, Suggested Method
(a)	16.0	−4.4	−22,900	−24,280
(c)	11.4	−5.0	−23,470	−23,580
(e)	5.4	−5.4	−22,770	−20,980
(g)	0	−5.5	−21,100	−18,600
(p)	−16.1	−5.1	−13,580	−15,400
(q)	−16.5	7.3	34,170	36,550
(s)	5.9	8.3	34,110	33,000
(u)	4.9	8.5	30,870	29,800
(w)	15.5	7.6	23,400	26,120

* x and y are measured from the principal axes to the centroids of elements as designated in Fig. 11.

The effects of the nacelle dead weight are substituted by hand-operated hydraulic "nacelle jacks," which apply down (tension) loads at the center of gravity of the nacelles through Chatillon traction dynamometers. The nacelle jack loads are applied to the test specimen through the wing-nacelle fittings.

The "lift jacks" act vertically upward, normal to the floor, and are distributed along the wing span so as to give the desired vertical bending moment M_L. The chordwise location determines the applied pitching moment. The "drag jacks" act upward, normal to the floor, on the bell cranks, which pull forward on cables attached to the wing. Fig. 14 shows a general view of the setup. The equipment is described in detail in reference 4.

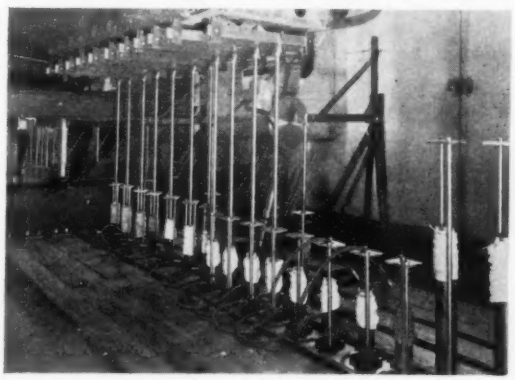

FIG. 14.

Lift and drag jacks operate on a common oil line. Since the friction in these specially designed jacks is negligible, the oil pressure in all jacks is the same; hence, the load applied by the jacks is proportional to the jack size and, in the case of the drag jacks, the bell-crank ratio.

This setup insures a simultaneous application of loads by all jacks. The setup is simple to operate and easy to oversee. The loading is accurate and easy to control. The specimen is readily accessible at all times and under all loadings. There are no inertia effects, and most of the danger and confusion resulting from secondary failures is eliminated.

Interpretation of Test Data

The test data include stress readings taken at seven Huggenberger stations as located in Fig. 9 for a series of 46 runs throughout a loading range of 0 to 725 lbs. per sq.in. hydraulic test pressure. From these data, straight-line load-stress curves are plotted for each Huggenberger station. For convenience, the applied load is given in terms of the hydraulic pressure in the jacks.

The actual stress distribution, curve Fig. 13, is plotted for an arbitrarily chosen applied test pressure of 700 lbs. per sq.in. by taking the stresses for each Huggenberger station from the corresponding load-stress curve.

CONCLUSIONS

The curves of stress distribution calculated according to the suggested method follow the shape of the measured stress distribution curves considerably better than the curves calculated by the standard method. By a better choice of the efficiency curves, the exact shape of the measured curve could be reproduced.

The actual values given by the new curve are, in general, too high, indicating that the estimation of effective areas, Fig. 11, is conservative for this new method of calculation.

The measured values in Fig. 13 for the upper rear and lower front corners are higher than the values calculated in both cases. Since the inclination of the calculated curves is due to the effect of bending in chordwise direction, the actual stresses due to the chordwise bending moment M_D are smaller than calculated. This indicates that the estimation of effective area with respect to chordwise bending is conservative and the effect of the trailing edge is not negligible.

It has therefore been demonstrated that curves of approximately identical numerical values and shapes as the measured curves can be calculated.

It is expected that a man of good judgment will be able, with some experience, to estimate effective areas and efficiency curves with reasonable accuracy, so that this method can be of considerable value in the practical design of efficient metal aircraft structures.

It is, however, highly desirable that reliable methods of estimating effective areas and efficiency curves be developed.

REFERENCES

[1] ANC-5, *Strength of Aircraft Elements*, Army-Navy-Commerce Committee on Aircraft Requirements, Washington, 1938.

[2] Wagner, Herbert, *Flat Sheet Metal Girders With Very Thin Metal Web, Parts I, II and III*, N.A.C.A. T.M. Nos. 604, 605 and 606, 1931.

[3] Kuhn, Paul, *Investigations on the Incompletely Developed Plane Diagonal-Tension Field*, N.A.C.A. T.R. No. 697, 1940.

[4] Tilgner, Charles, Jr., *Hydraulic Testing of Airplane Structures*, Aero Digest, Vol. 36, No. 1, p. 54, January, 1940.

Auditory Sensitivity Under Conditions of Anoxia: A Study of Speech Intelligibility*

C. P. SEITZ† AND G. M. SMITH‡
College of the City of New York

INTRODUCTION

NUMEROUS STUDIES CONCERNING the effects of oxygen deprivation on the organism have been undertaken. These studies (especially those of Heymens, Cobb, Gildea, McFarland and Evans, Seitz, and Seitz and Rosenthal) have implied that the nervous system is especially sensitive to lack of oxygen. The response of the eye has commonly served as the major indicator of decreased neural efficiency. There is reason to believe that the ear is also affected by oxygen deprivation in a similar manner. A survey of the literature, however, indicates that the observed effect of oxygen deprivation on the auditory threshold for pure tones is almost insignificant except at a relatively high altitude (20,000 ft., 9.53 per cent oxygen) and this, in spite of the fact that Wever and Bray have found marked reduction in the cochlear response following a restriction of the blood supply by pressure in the arteries.

In view of these facts and in view of the observed variability of the threshold for pure tones at high altitudes attributable to the distractions induced by an adjusting physiology (heart, breathing, etc.), it was throught advisable to work with sounds of speech complexity in the readily audible range.

PROBLEM

The purpose of the present study is to inquire into the effect of oxygen deprivation on the ability to perceive speech sounds in the easily audible range of stimulus intensities. It is obvious in dealing with this problem that two major variables are involved: (1) anoxia and (2) pressure. Pressure affects not only the availability of oxygen for the organism but also the ear and communication system in a mechanical sense. This exploratory study is restricted to oxygen deprivation uncomplicated by pressure changes.

METHOD AND MATERIALS

The method of observing the effect of oxygen deprivation was to note changes in the subjects' ability to perceive and report words in common speech. In order to obviate the possibility of the experimenter's attitude influencing his production of the speech stimuli, the test words were recorded. The recordings were made on 16-in. acetate discs with high-fidelity equipment. The stimuli were selected from test materials used by the Bell Telephone Laboratories[2] covering most of the sounds that occur in common speech. There were seven series of approximately 70 monosyllabic words each, for both the sea level and the altitude runs. The following combination were employed.

Test No.	Description
1	Single words
5	Words in groups of 2
2	Words in groups of 3
3	Words in groups of 4
4	Numbers in groups of 4
6	Words in groups of 2 plus range signals
7	Words in groups of 2 plus motor noises and range signals

The series were distributed so as to minimize the time factor, which is important because the effects of oxygen deprivation increase with prolonged exposure.

All of the experiments were carried out in the oxygen chamber of the College of the City of New York. The chamber is a solid room 8 ft. by 8 ft. by 7 ft. with walls approximately 8 in. thick making it relatively soundproof. An air-conditioning unit maintained the room at comfortable temperature and humidity. An altitude of 18,500 ft. (10.2 per cent oxygen) was simulated by running nitrogen into the chamber and diluting the air. This altitude was selected in order to have a condition that would be likely to yield unambiguous results. Though it is common practice to use oxygen above 10,000 or 12,000 ft., a pilot flying at 40,000 to 45,000 ft. breathing 100 per cent oxygen has a physiology roughly corresponding to that of a pilot at 16,000 to 18,000 ft. without oxygen.

Samples of the chamber air were taken after the ascent and subsequently analyzed on the Haldane-Henderson-Bailey gas analysis apparatus. None of the samples deviated more than the equivalent of 500 ft. from the desired altitude.

SUBJECTS

Sixteen male college students free from known systemic defects as determined by medical examination

Presented at Physiologic Problems Session, Tenth Annual Meeting, I.Ae.S., January 29, 1942.

* The authors acknowledge with appreciation a liberal grant of oxygen and nitrogen from the Linde Air Products Co.

† Instructor, Department of Psychology.

‡ Assistant Professor, Department of Psychology.

served as subjects. The age range was 17 to 25 with the median at 20 years.

Procedure

The subjects were examined individually under two separate conditions—sea level and altitude. Before the experiment proper began, brief instructions were given relative to the chamber and its use so as to allay any apprehension. The subject was then comfortably seated and a pair of Brush Communication Type Headphones* adjusted to the head. An instruction record with sample stimuli was then presented and the method of response was indicated—simple verbal repetition. The experimenter remained in the chamber with the subject to reassure him and also to record the responses on a check list. During the high-altitude run the experimenter was supplied with oxygen through a nasal catheter. The ascent took 27 min.; 15 min. were spent at altitude to allow for physiologic adjustment before any data were collected. Sea level and altitude runs were distributed so that each came first half of the time. The two forms of the test were also distributed so as to balance any inequality in difficulty.

Results

Table 1 gives results for each of the 16 subjects on tests 1, 2, 3, and 5 (tests without background noises) in terms of total errors. The total number of items was 280, of which 192 tested consonants and 88 vowels. It will be seen that in 12 out of 16 cases more errors were made at altitude than at sea level. The mean of the error ratios is 1.35, indicating a mean increase in errors of 35 per cent. The ratio of the means, a more stable value,† shows an increase in errors of 24 per cent. The individual differences in the error ratios are considerable, ranging from 2.44 to 0.55. Only four of these ratios are less than unity. It is interesting to observe that in all of these cases the easier form of the tests was taken at high altitude. Undoubtedly, some of the variability is a function of this unequal difficulty in the two forms of the tests. This inequality does not distort the results, however, since half of the subjects took the easier form at sea level and half at altitude. It is reasonable to suppose that a considerable part of the variability is due to individual differences in tolerance for low oxygen.

The data of Table 1, expressed in errors, become more meaningful if expressed in terms of articulation values for vowels, consonants, and standard syllables as in Table 2. In doing this the procedure of the Bell Laboratories was followed, where articulation value is defined as the per cent of stimuli correctly perceived. The consonant and vowel articulation were determined directly from our error data. The syllable articulations were calculated from the Bell Laboratory formula[2] derived empirically from extensive observations, $S = 1 - (1 - VC^2)^{0.9}$.

* The response curve of these phones cuts off sharply below 1,000 c.p.s. and is relatively flat (±10 decibel) from 1,000 to 8,000 c.p.s. Measurements were made at Stevens Institute of Technology. The transmission system as a whole was sufficiently free from gross distortions to make possible an easy identification of the speakers' voices.

† This ratio, obtained by dividing the sum of the errors at altitude by the sum of the errors at sea level, is less affected by extreme individual variations that enter into the calculation of the mean of the error ratios.

Table 1

The Effect of Altitude on Errors—Tests 1, 2, 3, 5, Combined

Subject	Sea Level	Altitude	Alt./S.L.
1	29 errors*	32	1.10†
2	22	46	2.09†
3	44	59	1.34
4	16	39	2.44
5	55	41	0.76†
6	38	21	0.55†
7	46	67	1.46
8	52	54	1.04
9	50	76	1.52
10	56	77	1.38†
11	49	43	0.88†
12	35	71	2.03
13	78	63	0.81†
14	55	61	1.11
15	46	87	1.89
16	52	60	1.15†
Mean	45.2	56.1	1.35
Ratio $M_{Alt.}/M_{S.L.}$	1.24		

* Total number of test items = 280 for each subject (192 consonants, 88 vowels).

† Easier form of test taken at altitude; in spite of this more errors were made at altitude in four of these eight cases.

Table 2

Articulation Values for Consonants, Vowels, and Standard Syllables—Tests 1, 2, 3, 5, Combined

	Sea Level			Altitude		
Subject	Consonant	Vowel	Syllable*	Consonant	Vowel	Syllable*
1	85.0%	100.0%	67.0%	85.0%	96.5%	65.0%
2	91.0	94.5	75.0	77.0	97.5	54.0
3	77.5	99.0	56.0	70.5	97.5	45.0
4	92.5	97.5	80.0	79.5	100.0	59.0
5	71.5	100.0	47.5	79.0	99.0	58.0
6	82.0	96.5	61.0	90.0	97.5	75.5
7	76.0	100.0	54.0	69.0	92.0	40.5
8	73.5	99.0	50.0	73.0	97.5	48.5
9	75.0	98.0	51.0	66.0	87.5	35.0
10	71.0	100.0	46.5	64.0	91.0	34.0
11	76.0	98.0	53.0	78.0	100.0	57.0
12	82.0	100.0	63.0	69.0	86.0	38.0
13	62.0	94.0	33.0	68.0	98.0	42.0
14	73.0	95.0	47.5	70.0	79.0	35.5
15	77.0	99.0	55.0	57.0	94.0	28.0
16	74.0	98.0	50.5	69.0	100.0	44.0
Mean	77.5	98.0	55.5	72.8	94.6	47.5
P.E.$_M$	1.25	0.33	1.98	1.13	0.49	3.33

* $S = 1 - (1 - VC^2)^{0.9}$.

As might be expected, consonants are less readily perceived than vowels at both sea level and altitude. The mean syllable articulation at sea level is 55.5 per cent; at high altitude it falls to 47.5 per cent. The reliability of the difference between these means was computed by Fisher's method for small correlated samples. The t value was 2.7, with a P value of 0.0082, indicating that the probability is less than 1 in 100 that the observed difference was due to chance.

Though the effect of altitude on syllable articulation may not seem impressive, an examination of Fig. 1 re-

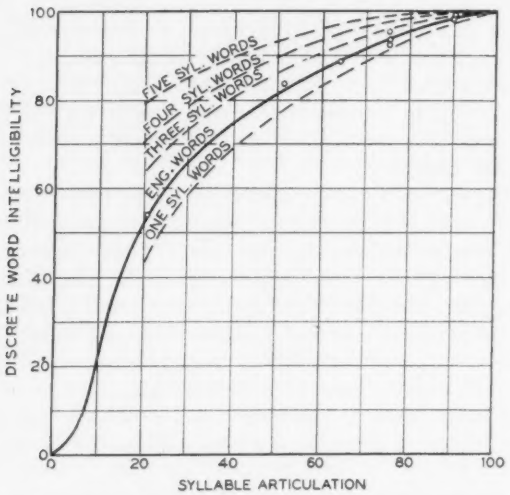

FIG. 1. Di crete word intelligibility vs. syllable articulation. (Reproduced from Bell Telephone Laboratory Bulletin B-436, with the permission of the author.)

produced from the report of Fletcher and Steinberg[2] will show that a loss in intelligibility of this magnitude may be critical for word intelligibility. This figure shows the relationship between syllable articulation and single word intelligibility. A critical point is reached in the neighborhood of 30 per cent syllable articulation, where a slight change in syllable articulation corresponds to a much larger change in word intelligibility. No communication system gives perfect intelligibility under conditions of flight because of noise, vibration, and low pressure. Any additional factors such as anoxia or poor speech production may reduce articulation to the critical point.

The results based upon our two tests with background noises are mentioned with some diffidence because it was felt that the experimental procedure that lies back of them was based on inadequate equipment. However, the procedure did have exploratory value and the results suggest further lines for investigation. There was a marked drop in consonant, vowel, and syllable articulation as might have been anticipated, the mean syllable articulation values being reduced to about 20 per cent. The altitude effect was small but consistent with the results for the tests without background noises.

It is noteworthy that no errors were made in the number series at either sea level or altitude. This is to be expected since numbers can be identified from the vowel sounds alone and it will be recalled that vowel articulation was 98 per cent at sea level and 95 per cent at altitude. This is of considerable importance in working out codes such as are now being adopted in military and civil aviation in order to comply with restrictions imposed by wartime conditions.

REFERENCES

[1] Cobb, S., *A Preface to Nervous Disease*, 173 pp.; W. Wood & Co., Baltimore, 1936.

[2] Fletcher, H., and Steinberg, J. C., *Articulation Testing Methods*, Bell Telephone Laboratories, pp. 41, 42, 46; Reprint B-436, November, 1929.

[3] Gildea, E. F., and Cobb, S., *The Effects of Anemia on Cerebral Cortex of the Cat*, Arch. Neurol. & Psychiat., Vol. 23, pp. 876–903, 1930.

[4] Heymens, C., and Bouckaert, J. J., *Sur la Survie et la Reanimation des Centres Nerveau*, Compt. rend. Soc. de biol., Vol. 119, p. 324, 1935.

[5] McFarland, R. A., and Evans, J. N., *Alterations in Dark Adaptation Under Reduced Oxygen Tension*, Am. J. Physiol., Vol. 127, pp. 37–50, 1939.

[6] Seitz, C. P., *The Effects of Anoxia on Visual Function*, Arch. Psychol., Vol. 36, No. 257, August, 1940.

[7] Seitz, C. P., and Rosenthal, C. M., *The Effect of Oxygen Deprivation and Strychnine Administration on Visual Function*, Arch. Ophth., Vol. 26, pp. 276–287, August, 1941.